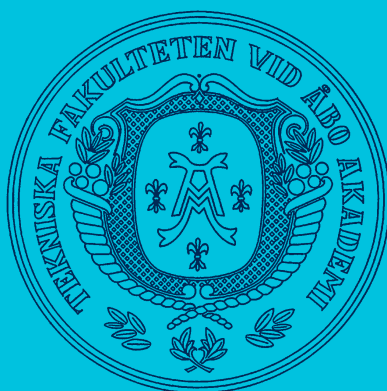


SYNTHESIS, CHARACTERIZATION AND CHEMICAL SENSOR APPLICATION OF CONDUCTING POLYMERS

Michał Wagner



Laboratory of Analytical Chemistry
Process Chemistry Centre
Department of Chemical Engineering
Åbo Akademi University

Åbo/Turku, Finland
2013

SYNTHESIS, CHARACTERIZATION AND CHEMICAL SENSOR APPLICATION OF CONDUCTING POLYMERS

Michał Wagner



*Laboratory of Analytical Chemistry
Process Chemistry Centre
Department of Chemical Engineering
Åbo Akademi University*

*Åbo/Turku, Finland
2013*

Supervisors

Professor Carita Kvarnström
Laboratory of Materials Chemistry and Chemical Analysis
University of Turku

Professor Ari Ivaska
Laboratory of Analytical Chemistry
Åbo Akademi University

Professor Johan Bobacka
Laboratory of Analytical Chemistry
Åbo Akademi University

Reviewer

Professor Csaba Visy
Institute of Physical Chemistry
University of Szeged
Hungary

Reviewer and Opponent

Professor Alexander Kuhn
Institute of Molecular Sciences
University of Bordeaux
France

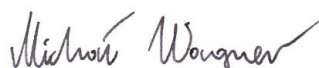
Preface

The research work summarized in this thesis was mainly carried out at the Laboratory of Analytical Chemistry of Åbo Akademi University. I would like to thank the following institutions for financial support: Graduate School of Materials Research, National Graduate School in Nanoscience, Research Foundation for Åbo Akademi, The Finnish Funding Agency for Technology and Innovation, Academy of Finland and Australian National Fabrication Facility.

For the scientific support and the opportunity to study at Åbo Akademi, my three supervisors are gratefully acknowledged. Carita, Ari and Johan, *tack så mycket!* for your suggestions and many discussions that lead to the interesting findings shown in this work. Also I would like to thank all the co-authors of my scientific articles for their contributions as well the reviewers of my thesis (Prof. Csaba Visy and Prof. Alexander Kuhn) for having patience to evaluate this work.

Special thanks for my friends in Åbo! You have made my stay in Finland really joyful. Thank you! Grzesiek, Weronika, Dorota, Patrycja, Ting Ting, Ulrika, Neg, ... and this list could continue forever!

Finally, I want to thank my beloved family. Dziękuję wam za bezgraniczne wsparcie i miłość!!! This work is dedicated to you.



Åbo, October 2013

“Per Aspera ad Astra”

Abstract

Polymeric materials that conduct electricity are highly interesting for fundamental studies and beneficial for modern applications in *e.g.* solar cells, organic field effect transistors (OFETs) as well as in chemical and bio-sensing. Therefore, it is important to characterize this class of materials with a wide variety of methods. This work summarizes the use of electrochemistry also in combination with spectroscopic methods in synthesis and characterization of electrically conducting polymers and other π -conjugated systems. The materials studied in this work are intended for organic electronic devices and chemical sensors. Additionally, an important part of the presented work, concerns rational approaches to the development of water-based inks containing conducting particles.

Electrochemical synthesis and electroactivity of conducting polymers can be greatly enhanced in room temperature ionic liquids (RTILs) in comparison to conventional electrolytes. Therefore, poly(para-phenylene) (PPP) was electrochemically synthesized in the two representative RTILs: bmimPF₆ and bmtf₂N (imidazolium and pyrrolidinium-based salts, respectively). It was found that the electrochemical synthesis of PPP was significantly enhanced in bmimPF₆. Additionally, the results from doping studies of PPP films indicate improved electroactivity in bmimPF₆ during oxidation (p-doping) and in bmtf₂N in the case of reduction (n-doping). These findings were supported by in situ infrared spectroscopy studies.

Conducting poly(benzimidazobenzophenanthroline) (BBL) is a material which can provide relatively high field-effect mobility of charge carriers in OFET devices. The main disadvantage of this n-type semiconductor is its limited processability. Therefore in this work BBL was functionalized with poly(ethylene oxide) PEO, varying the length of side chains enabling water dispersions of the studied polymer. It was found that functionalization did not distract the electrochemical activity of the BBL backbone while the processability was improved significantly in comparison to conventional BBL.

Another objective was to study highly processable poly(3,4-ethylenedioxythiophene) poly(styrenesulfonate) (PEDOT:PSS) water-based inks for controlled patterning scaled-down to

nearly a nanodomain with the intention to fabricate various chemical sensors. Developed PEDOT:PSS inks greatly improved printing of nanoarrays and with further modification with quaternary ammonium cations enabled fabrication of PEDOT:PSS-based chemical sensors for lead (II) ions with enhanced adhesion and stability in aqueous environments. This opens new possibilities for development of PEDOT:PSS films that can be used in bio-related applications.

Polycyclic aromatic hydrocarbons (PAHs) are a broad group of π -conjugated materials consisting of aromatic rings in the range from naphthalene to even hundred rings in one molecule. The research on this type of materials is intriguing, due to their interesting optical properties and resemblance of graphene. The objective was to use electrochemical synthesis to yield relatively large PAHs and fabricate electroactive films that could be used as template material in chemical sensors. Spectroscopic, electrochemical and electrical investigations evidence formation of highly stable films with fast redox response, consisting of molecules with 40 to 60 carbon atoms. Additionally, this approach in synthesis, starting from relatively small PAH molecules was successfully used in chemical sensor for lead (II).

Referat

Elektriskt ledande polymerer är mycket intressanta material både med tanke på fundamental forskning och moderna tillämpningar t.ex. i solceller, organiska transistorer (OFET) samt i kemiska och biosensorer. Därför är det mycket viktigt att karakterisera dessa material med olika analytiska tekniker. I detta arbete används elektrokemiska metoder och deras kombinationer med vissa spektroskopiska metoder för karakterisering av elektriskt ledande polymerer och andra π -konjugerade system. Material som har studerats i detta arbete finner användning närmast i organiska elektroniska komponenter och kemiska sensorer. I detta arbete behandlas ytterligare utveckling av ett vattenbaserat bläck som består av elektriskt ledande polymerer.

Elektrokemisk syntes av ledande polymerer kan också utföras i joniska vätskor vid rumstemperatur (RTIL) i vilka ledande polymerer generellt även har funnits visa höjd elektroaktivitet. Därför studerades elektrokemisk syntes av poly(parafenylen) (PPP) i två olika joniska vätskor: bmimPF_6 och bmiTf_2N (på imidazolium och pyrrolidinium baserade salter). Elektrokemisk syntes av PPP i bmimPF_6 förbättrades avsevärt jämförd med syntes i organiska lösningsmedel. Då dopningsreaktioner av PPP studerades i dessa joniska vätskor fann man, att polymerens p-dopning i bmimPF_6 och n-dopning i bmiTf_2N förbättrades avsevärt. Dessa resultat kunde bekräftas med in situ IR-spektroskopiska studier.

Det elektrisk ledande materialet poly(benzimidazobenzofenantrolin) (BBL) visar relativt hög fälteffekt-mobilitet av laddningsbärare och kan med fördel användas i OFET-komponenter. Nackdelen med BBL som är en n-typs halvledare är dess begränsade processbarhet. I detta arbete studerades möjligheten att funktionalisera BBL med olika långa sidokedjor av poly(ethylenoxid) (PEO). På detta sätt kunde man framställa vattendispersioner av BBL. Funktionaliseringen påverkade inte BBLs elektroaktivitet med däremot ökade dess processbarhet avsevärt jämfört med icke-funktionaliserat BBL.

I detta arbete utvecklades också kompositmaterial av poly(3,4-etylendioxytiofen)-poly(styrenulfonat) (PEDOT:PSS) för användning som ledande bläck. Detta material skulle

användas vid framställning av olika kemiska sensorer i nanoskala. Det utvecklade PEDOT:PSS-bläcket visade sig ha goda egenskaper för tryckning av nanomönster. Då bläcket modifierades ytterligare med kvartära ammoniumjoner, kunde man framställa kemiska sensorer för bly(II)joner. Materialet visade också ökad adhesion till substratet och stabilitet i vattenlösningar. Detta öppnar nya möjligheter för användning av membraner bestående av PEDOT:PSS i biologiska tillämpningar.

Polycykliska aromatiska kolväten (PAH) är en bred grupp av π -konjugerande material som består av olika antal aromatiska ringar, från naftalen till molekyler som består av flera hundra ringar. Forskning av dessa material är av stort intresse, inte minst av att de påminner grafen till sin struktur. Målet med denna del av avhandlingen var att använda elektrokemisk syntes för framställning av relativt stora PAH-molekyler som skulle användas i kemiska sensorer. Spektroskopiska, elektrokemiska och elektriska studier visade att man kunde framställa mycket stabila membraner med snabba redox-förlopp. Dessa molekyler bestod av 40 till 60 kolatomer. Relativt små PAH-molekyler framställda på detta sätt kunde användas med fördel i kemiska sensorer för bly(II)joner.

The thesis is based upon the following papers:

- I. Michal Wagner, Carita Kvarnström and Ari Ivaska, "Room temperature ionic liquids in electrosynthesis and spectroelectrochemical characterization of poly(paraphenylene)" *Electrochimica Acta*, 55 (2010) 2527–2535.
- II. Michal Wagner, Anna Österholm, Sami-Pekka Hirvonen, Heikki Tenhu, Carita Kvarnström and Ari Ivaska, "Characterization of water dispersible n-type poly (benzimidazobenzo-phenanthroline) BBL derivatives", *Macromolecular Chemistry and Physics*, 212 (2011) 1567–1574.
- III. Michal Wagner, Kai Yu, Carita Kvarnström and Ari Ivaska, "Synthesis and characterization of electroactive films based on benzo(a)pyrene", *Electrochimica Acta*, 56 (2011) 3443–3446.
- IV. Michal Wagner, Carita Kvarnström, Ari Ivaska and Johan Bobacka, "Electrochemical properties of novel porous carbon based material synthesized from polycyclic aromatic hydrocarbons", *Electrochimica Acta*, 105 (2013) 384–393.
- V. Grzegorz Lisak, Michal Wagner, Carita Kvarnström, Johan Bobacka, Ari Ivaska, and Andrzej Lewenstam, "Electrochemical behaviour of poly(benzopyrene) films doped with eriochrome black T as a Pb^{2+} -selective sensors", *Electroanalysis*, 22 (2010) 2794–2800.
- VI. Michal Wagner, Grzegorz Lisak, Ari Ivaska and Johan Bobacka, "Durable PEDOT:PSS films obtained from modified water-based inks for electrochemical sensors", *Sensors and Actuators B*, 181 (2013) 694–701.
- VII. Michal Wagner, Cathal D. O'Connell, David G. Harman, Ryan Sullivan, Ari Ivaska, Michael J. Higgins and Gordon G. Wallace, "Synthesis and optimization of PEDOT:PSS based ink for printing nanoarrays using Dip-Pen Nanolithography", accepted manuscript in *Synthetic Metals*.

Note: all of the papers listed above are re-printed in the appendix with a permission of the copyright holders.

Contributions of the author:

Papers I and IV. The author performed all the experimental work, evaluated all the results, and wrote the manuscript.

Papers II, V, VI and VII. The author performed the experimental work, evaluated the results, and wrote the manuscript together with the co-authors.

Paper III. The author evaluated all the results and wrote the manuscript. The experimental work was performed together with the co-authors.

Table of contents

1. A brief introduction to electrically conducting polymers.....	1
2. Essential aspects of conducting polymers.....	2
2.1. Electronic structures and charge transfer.....	2
2.2. Optical properties.....	9
2.3. Chemical and electrochemical synthesis.....	12
3. Selected applications of conducting polymers.....	15
3.1. Organic electronics.....	15
3.2. Chemical sensors and biosensors.....	17
4. New monomers and electrolytes for electrochemical synthesis of electroactive materials.....	20
4.1. Polycyclic aromatic hydrocarbons.....	20
4.2. Room temperature ionic liquids.....	22
5. Synthesis, characterization and deposition techniques of studied electroactive films.....	25
5.1. Cyclic voltammetry.....	25
5.2. Molecular spectroscopy.....	27
5.3. Electrochemical impedance spectroscopy.....	30
5.4. Electrical conductivity and in-situ conductance measurements.....	33
5.5. Potentiometric measurements.....	35
5.6. Surface characterization and deposition at nanoscale.....	37
6. Results and discussion.....	40
6.1. Electrochemistry of poly(para-phenylene) in room temperature ionic liquids.....	40
6.2. Investigation of the water-soluble conducting polymer BBL derivatives.....	45
6.3. Synthesis, structure and electrochemistry of novel conducting films based on polycyclic aromatic hydrocarbons.....	48
6.4. Development of water-based PEDOT:PSS inks for nanoprinting and durable chemical sensors ..	56
7. Final summary and possible future directions.....	65
List of references.....	66

List of abbreviations and symbols

AC	alternating current
ACN	acetonitrile
AFM	atomic force microscopy
ATR	attenuated total reflectance
A	surface area of a WE (cm^2)
a_p	activity of the primary ion (M)
a_i	activity of the interfering ion (M)
a_{x1}	activity of the primary ion outside a membrane (M)
a_{x2}	activity of the primary ion inside a membrane (M)
BaP	benzo(a)pyrene
BBL	poly(benzimidazobenzophenanthroline)
bmimPF ₆	1-butyl-3-methylimidazolium hexafluorophosphate
bmpTf ₂ N	1-butyl-1-methylpyrrolidinium bis(trifluoromethylsulfonyl)imide
B	time constant related to diffusion ($\text{s}^{1/2}$)
CE	counter electrode
CPE	constant phase element
CTA ⁺	hexadecyltrimethylammonium cation
CV	cyclic voltammetry
C	capacitance (F)
C_{dl}	double layer capacitance (F)
c_b	bulk concentration (mol cm^{-3})
c_p	concentration of the primary ion (M)
c_i	concentration of the interfering ion (M)
DC	direct current
DNA	deoxyribonucleic acid
DPN	dip-pen nanolithography
DSC	dye sensitized solar cell
D	diffusion coefficient ($\text{cm}^2 \text{s}^{-1}$)
d_h	density of holes (cm^{-3})
d_e	density of electrons (cm^{-3})
d_f	density of a film (g cm^{-3})
d_p	penetration depth (in units of length)
EbT	eriochrome black T
EDX	energy-dispersive X-rays
EG	ethylene glycol
EIS	electrochemical impedance spectroscopy
E	electrical potential (V)
E_{cell}	total potential of electrochemical cell/battery (V)
$E^{\circ'}$	formal redox potential (V)
E_{ox}	oxidation potential (V)
E_{red}	reduction potential (V)
E_p	peak-to-peak separation (V)
E_v	energy of oscillator (Hz)
emf	electromotive force (V)
FET	field-effect transistor
FTIR	Fourier transform infrared spectroscopy

<i>F</i>	Faraday constant (equal to 96485 C mol ⁻¹)
<i>f_c</i>	force constant (N m ⁻¹)
GC	glassy carbon substrate
<i>G</i>	electrical conductance (S)
HOMO	highest occupied molecular orbital
IR	infrared
IRAV	infrared active vibration
ISE	ion-selective electrode
ISM	ion-selective membrane
ITO	indium tin oxide
<i>I</i>	electrical current (A)
<i>I_d</i>	intensity of the “d” band
<i>I_g</i>	intensity of the “g” band
<i>I_p</i>	peak current (A)
<i>I_t</i>	intensity of transmitted light
<i>I₀</i>	intensity of incident photons
<i>J</i>	current density (A cm ⁻²)
<i>K_{p,i}</i>	selectivity coefficient
<i>k_s</i>	constant number equal to 269000
LUMO	lowest unoccupied molecular orbital
LED	light-emitting diode
<i>LDL</i>	lower detection limit (M)
<i>L_a</i>	crystallite length (nm)
<i>L_b</i>	length of the double-band electrode (cm)
<i>L_f</i>	film thickness (μm)
<i>L_s</i>	light path (cm)
<i>L_{sb}</i>	length of the half spacing of the double-band electrode (nm)
<i>M_m</i>	molecular weight of a monomer (g mol ⁻¹)
<i>m_r</i>	reduced mass (kg)
<i>n</i>	the value in between or equal to 0 and/or 1 (related to CPE)
<i>n_e</i>	number of transferred electrons
<i>n_n</i>	refractive index
OSC	organic solar cell
OTFT	organic thin-film transistor
O	hyperbolic cotangent diffusion element
PA	polyacetylene
PAH	polycyclic aromatic hydrocarbon
PANI	polyaniline
PBP	poly(benzopyrene)
PC	propylene carbonate
PEDOT	poly(3,4-ethylenedioxythiophene)
PEO	poly(ethylene oxide)
PF	polyfluorene
PPP	poly(para-phenylene)
PPy	polypyrrole
PPV	poly(para-phenylenevinylene)
PSS	poly(styrenesulfonate)
PT	polythiophene

PVC	poly(vinyl chloride)
QAB	quaternary ammonium bromide
Q	electric charge (C)
Q_p	polymerization charge (C)
Q_d	doping charge (C)
q_c	charge of carrier (C)
q_p	charge number of the primary ion
q_i	charge number of the interfering ion
RE	reference electrode
RTIL	room temperature ionic liquid
R_e	equilibrium distance (in units of length)
R_f	film resistance (Ω)
R_p	polarization resistance (Ω)
R_s	solution resistance (Ω)
R	ideal gas constant (equal to $8.3144621 \text{ J mol}^{-1} \text{ K}^{-1}$)
SEM	scanning electron microscopy
S_n	energy level of a singlet state ($n = 0, 1, 2, \dots$)
TBA^+	tetrabutylammonium cation
TBAPF_6	tetrabutylammonium hexafluorophosphate
TMOA^+	trimetyloctylammonium cation
TOA^+	tetraoctylammonium cation
T	hyperbolic tangent diffusion element
T	temperature (K)
t	time (s)
UV-vis	ultraviolet and visible
v	scan rate (V s^{-1})
ν_n	vibrational quantum numbers ($n = 0, 1, 2, \dots$)
WE	working electrode
W	work (J)
Y_0	magnitude of admittance ($\text{S s}^{1/2}$ or S s^n depending on the type of electrical element)
Z	electrical impedance (Ω)
Z'	real part of the impedance (<i>i.e.</i> resistance) (Ω)
Z''	imaginary part of the impedance (<i>i.e.</i> reactance) (Ω)

Greek-based symbols

γ_f	attenuation coefficient (cm^{-1})
γ_p	activity coefficient
θ	phase angle
μ_h	mobility of holes ($\text{cm}^2 \text{ V}^{-1} \text{ s}^{-1}$)
μ_e	mobility of electrons ($\text{cm}^2 \text{ V}^{-1} \text{ s}^{-1}$)
σ	electrical conductivity (S cm^{-1})
ρ	resistivity ($\Omega \text{ cm}$)
χ^2	fitting error
ω	angular frequency (rad s^{-1})

Note: the metric prefixes for some of the units and their dimensions were chosen arbitrarily.

1. A brief introduction to electrically conducting polymers

Until the discovery of the significant increase in electrical conductivity during oxidation of polyacetylene (PA) with iodine vapor in 1977 [1], all polymers were commonly regarded as electrical insulators. The first work on truly conducting polypyrrole (PPy) oxidized with iodine emerged already in 1963 [2], however, this work did not acquire immense attention from the scientific community. Thus the era of conducting polymers originates from studies on trans-PA oxidized with iodine, covering the whole range of electrical conductivity: from insulating state to metal-like behavior [1,3]. Due to numerous highly important reports in both fundamental and applied research, conducting polymers were recognized by the Nobel committee in 2000 [4]. The excitement over conducting polymers can be attributed to the fact that in principle they constitute a new branch of materials which binds together desired semiconducting properties with mechanical flexibility and in some cases biocompatibility. Such a highly practical combination is not observed in metals, inorganic semiconductors or non-conjugated saturated polymers. Also, the advent of conducting polymers created new opportunities for fundamental studies in solid-state physics and actually this type of materials are another fascinating crossover of chemistry and physics.

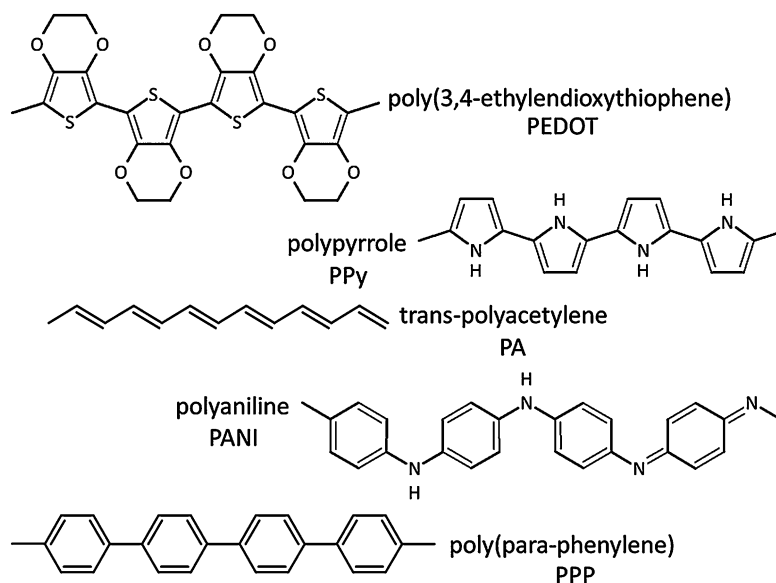


Figure 1. Chemical structures of common conducting polymers.

The structure of conducting polymers is usually composed of C, H and heteroatoms like N or S within a π -conjugated system. Figure 1 presents the basic chemical structure of some conducting polymers. Delocalized π -electrons originate from one unpaired electron per carbon atom in contrary to saturated polymers where all four valence electrons are used to constitute covalent chemical bonds. What all conducting polymers have in common is a high π -electron overlap along the polymer chain which facilitates the possibility of fast electron transfer. Despite of that fact, delocalization of π -electrons along the polymer backbone itself is not sufficient to obtain high conductivities and a process called doping is needed. Chemically this process is related to oxidation/reduction of the polymer, resulting in formation of charge carriers. Importantly the behavior of those charge carriers can be in depth explained by solid-state physics. Hence, conducting polymers were also used as model compounds in studying *e.g.* electron-lattice interactions [5] or Mott insulator/metal transition [6]. Since conducting polymers can easily be chemically or electrochemically doped, it is possible to incorporate ions into polymer films that can carry desired functionality. This fact facilitated numerous ideas in designing new devices and real applications *e.g.* in corrosion science, organic electronics, energy storage and chemical sensors [7-10].

2. Essential aspects of conducting polymers

2.1. Electronic structures and charge transfer

In nature, energy that systems possess can be quantized into small portions which can be visualized as energy levels. In every atom, electrons occupy certain energy levels and they cannot be found in between the energy gap (difference in two energy states). In other words electrons can adopt only specific orbitals with specific energies. From the chemical point of view, important are relations and configurations of electrons from the outermost electron shell (valence electrons), since they contribute to chemical bonds between atoms. Interactions of atoms result in formation of molecules and thus the probability of finding an electron in a specific space-time domain can be calculated using the concept of molecular orbital. Many physical and chemical properties of condensed matter can be accurately described by the band theory of solids. The bands are a visualization of overlapping of many molecular orbitals where

energy can be considered as continuous. According to this theory, valence electrons are statistically attributed to the so-called valence band and virtually free electrons with higher energies to the conduction band.

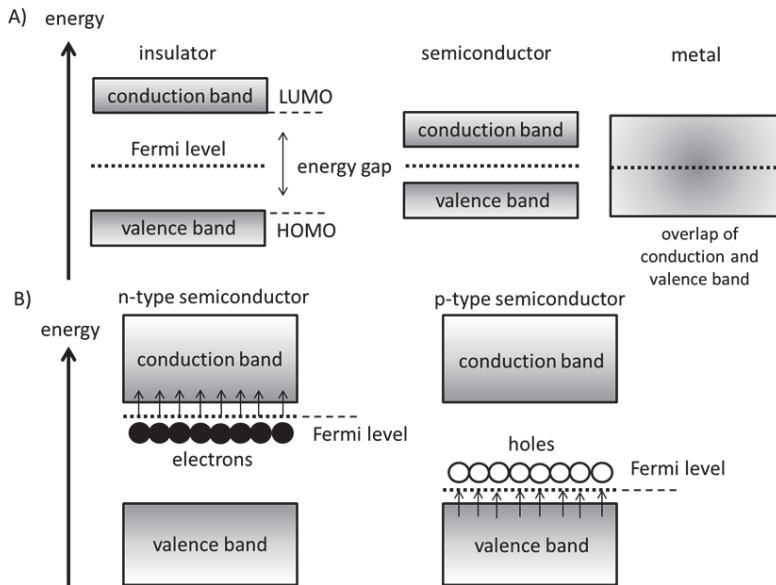


Figure 2. The band structures of three conductivity classes of materials as a function of energy at 0 K (A). Simplified representation of doping mechanism for inorganic semiconductor shown as a function of energy (B).

When considering the flow rate of electrons through solid matter, all known materials can be divided into three groups: insulators, semiconductors and conductors. Those groups can be interpreted in terms of the band theory yielding satisfactory explanations for many physical and chemical phenomena. Upon thermal or other excitations, electrons change their state and “jump” to energy levels with higher quantum numbers. According to Fermi-Dirac statistics all electrons are in constant movement even at 0 K and at this temperature will fill all available energy states below a certain energy level termed the Fermi level. For insulators and semiconductors at 0 K, the Fermi level appears exactly in between the valence and conduction bands. What makes a semiconductor different from insulator is the significantly smaller energy of the band gap of the former. Hence, for a semiconductor at higher temperatures this threshold energy can statistically be overcome by electrons (extension of Fermi level). In a

conductor like metal, valence electrons are essentially free and the conduction and valence band is merged, and split in half by Fermi level at 0 K. Figure 2 A presents three conductivity classes according to the band theory and the lowest unoccupied molecular orbital (LUMO) and the highest occupied molecular orbital (HOMO) also marked in the figure.

Electrical conductivity depends on structural arrangement of matter, *i.e.* crystalline vs. disordered systems. For metals which possess crystalline structure the conductivity decreases with increasing temperature and at high temperatures this relation is linear. This increase in electrical resistance is mostly due to the scattering of electrons by interactions with phonons (in this case: thermally induced vibrations of the crystalline lattice). In a simplified view on semiconductors, the rise in temperature facilitates formation of excited electrons which can move from the valence band to the conduction band. Hence, the electrical resistance of a semiconductor decreases exponentially with increasing temperature. The removal of electrons from the valence band produces virtual charge carriers: electron holes. Hence, the overall conductivity of a semiconductor is in general, dependent on the charge, mobility and density of the carriers, according to the following equation:

$$\sigma = q_c(d_h\mu_h + d_e\mu_e) \quad (1)$$

Where: σ is the electrical conductivity in $S\text{ cm}^{-1}$, q_c is the charge of carrier in C. The symbols $\mu_{(h,e)}$ and $d_{(h,e)}$ refer to charge carrier mobility in $\text{cm}^2\text{ V}^{-1}\text{ s}^{-1}$ and density in cm^{-3} , with respect to holes (h) and electrons (e). As can be seen from equation 1, the mobility of charge carriers in an electric field, plays a dominant role in the conductivity of semiconductors and with increasing order the movement of charge carriers can be significantly enhanced.

Both inorganic and organic semiconductors can be doped, creating defects that have influence on the order of the system. The simplified effect of doping on the electronic structure of an intrinsic inorganic semiconductor can be seen in Figure 2 B. Insertion of *e.g.* arsenic or boron atoms into the crystalline structure of silicon creates defects that can be visualized by an additional energy level. Doping of silicon with arsenic creates an electron donor level near the conduction band (left picture in Figure 2 B). Free electrons from an electron donor propagate

to the conduction band by passing an energy barrier that is significantly smaller than energy band gap between the conduction and valence band. Since charge carrier movement is described by negative electrons this donor doped material is referred to as an n-type semiconductor. On the other hand, doping of silicon with boron creates an electron acceptor level near the valence band (right picture in Figure 2 B). Electrons from the valence band propagate to the acceptor level which has electron deficiency, leaving positive holes in the valence band propagating in opposite direction and thus this acceptor doped material is referred to as a p-type semiconductor.

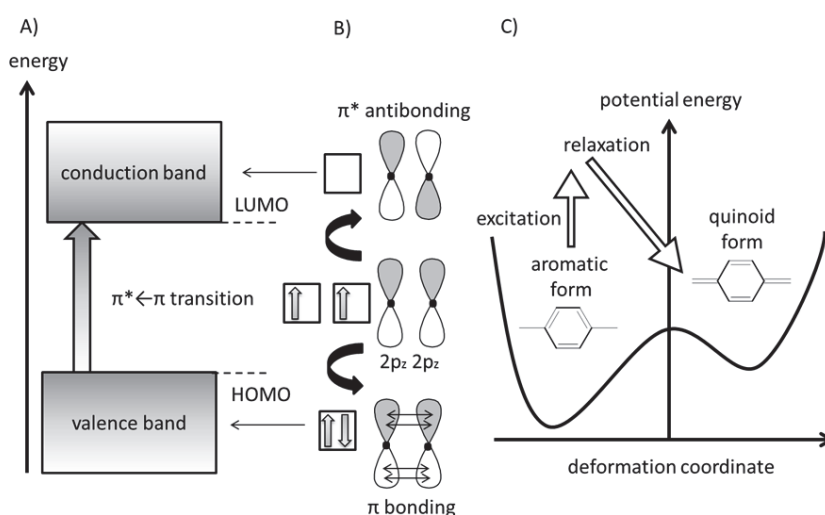


Figure 3. Simplified band structure of neutral conducting polymer as a function of energy (A). The formation of π bonding and antibonding orbitals between two carbon atoms in the polymer backbone (B). Note: the phase of the wavefunction in $2p_z$ orbitals is marked with gray and white colors. Potential energy vs. configuration forms (benzenoid and quinoid) of PPP as an example (C).

The neutral state of conducting polymers is presented in Figure 3 A. Since all conducting polymers have a conjugated π -electron system, the fundamental optical transition is between the bonding (π) and antibonding (π^*) molecular orbitals. In principle, delocalized electrons in organic compounds originate from overlap of $2p_z$ orbitals (p-orbitals oriented in z-direction). When two $2p_z$ orbitals overlap the newly formed orbital is split into two levels with different energies according to Pauli exclusion principle (Figure 3 B). Conducting polymers tend to create

an amorphous microstructure without long-range order. Hence, the conjugation range of π orbitals is limited and a “short” conjugation is specific for conducting polymers resulting in potential barriers. When additional energy is delivered to the system along the polymer backbone, an exciton (new state of an electron and hole) is formed. In trans-PA excitation leads to formation of new a quasi-particle that has its electronic state in the middle of the band gap, termed soliton [11,12]. Physically soliton is an isolated propagating wave that does not disperse. The formation of solitons in trans-PA originate from the fact that this conducting polymer possess two structures with equal energy in the ground state (degeneration). For other conducting polymers, excitation leads to essentially different chain distortions. An example of two energetically non-equal chemical structures of PPP is shown in Figure 3 C: the stable aromatic structure and the quinoid meta-stable one with a higher local energy minimum. After excitation, the polymer relax to the meta-stable energy states since this process is relatively faster than relaxation to the aromatic configuration [12]. Such a chain distortion is equivalent to a quasi-particle termed polaron which physically is a moving electron or hole with surrounding deformation. During redox reactions of conducting polymers polarons or bipolarons are formed.

The band structures of distorted polymer chains and corresponding chemical equivalents are shown in Figure 4. When conducting polymer is oxidized, electron is removed from the polymer chain leaving a positively charged hole which can propagate along the chain (Figure 4 A). In other words, an ionized stable quinoid form of the conducting polymer is generated with coupled charged and neutral defects. In order to preserve electroneutrality of the system, the newly formed charge carrier needs to be counterbalanced with an anion. From a physical point of view new energy levels are formed in the band structure and Fermi level is located close to the valence band. In some cases (*e.g.* “heavier” doping) two charge carriers are formed and they are counterbalanced with two anions (Figure 4 B). This chain deformation is traditionally called bipolaron with energy levels closer to the mid energy gap than the polaron. The major difference between polaron and bipolaron is the spin. The polaron spin is equal to $\frac{1}{2}$ in contrast to the bipolaron which is spinless. Chemically, the positive polaron and bipolaron are referred to as radical cation and radical dication respectively. Figure 4 C and D show the electronic and

chemical structure of a conducting polymer in reduced form. Addition of electrons yields formation of negative polarons and bipolarons. The negative charges are counterbalanced with cations. For those systems Fermi level is located close to the conduction band. In analogy to the oxidized polymer, negative polarons and bipolarons refer to radical anions and radical dianions, respectively.

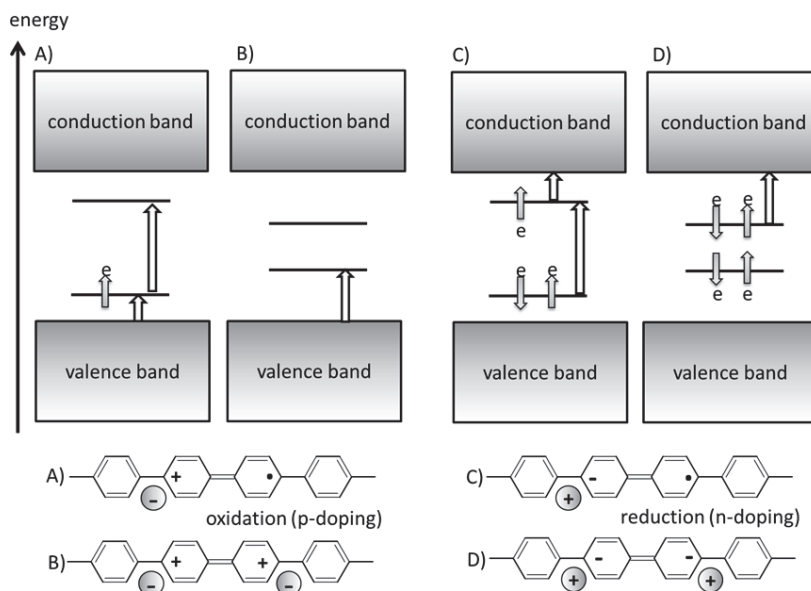


Figure 4. Simplified representation of band structures in excited conducting polymers as a function of energy, together with corresponding chemical structures shown for PPP as an example. Notes: the direction of gray arrows represents electron spin and white arrows denote allowed optical transitions.

There are essential differences in conduction and doping mechanisms between organic and inorganic semiconductors, due to already mentioned absence of long-range order within π -conjugated systems. The absence of long-range order in organic semiconductors leads to much lower carrier mobilities in comparison to metals or inorganic semiconductors. Interestingly, even for the highest reported carrier mobility for polythiophenes (PTs) in field-effect transistors the corresponding free path at room temperature of the carrier is lower than the interatomic distance [13].

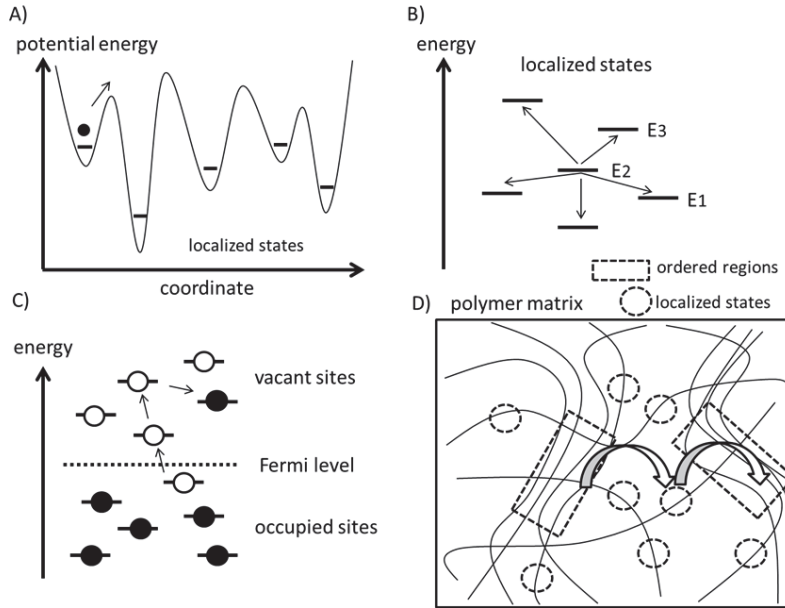


Figure 5. Schematic representation of localized states in disordered systems as a function of potential energy (A). Charge carrier hopping to different localized states with different energies (B) and near Fermi level at temperatures higher than 0 K (C). Schematic picture of disordered and crystalline regions in conducting polymer (D). Note: the electrical coupling between crystalline regions is shown with white arrows.

Figure 5 A presents a charge carrier propagating in a disordered system. The periodic potential energy distribution is disturbed leading to the absence of delocalized wave functions and formation of localized states (in this case “traps” for the carrier). Essentially, trapped charge carriers have zero mobility. On the other hand, carriers can “jump” to from one localized state to another *via* hopping/tunneling effects. Statistically, carrier can “jump” to the nearest localized energy states (Figure 5 B). Hopping of a carrier from *e.g.* state E_2 to E_1 is easier than hopping to the state E_3 , however, both transitions contribute to the rate of carrier jumps. The “jumps” between localized states can be described by models based on variable range hopping. In disordered hopping systems localized states are distributed randomly in space and energetically distributed in accordance with density of states function [14]. In principle, density of states describes all the states at each energy level that can be potentially occupied. Figure 5 C presents a schematic sketch of random hopping of charge carriers near the Fermi level at temperatures higher than 0 K. For conducting polymers only the small fraction of dopants

leads to charge carriers taking part in the hopping transport in contrary to inorganic semiconductors, due to the fact that only the localized states near the Fermi level can be considered. However, the significant increase in dopant concentration leads also to increase in density of states promoting a higher hopping rate because of the reduced distance between the localized states.

An overall electrical conductivity of common conducting polymers can be tuned to the range of 10^2 - 10^3 S cm⁻¹ [15,16]. Such high conductivity values are only approximately two orders of magnitude lower than for copper at room temperature. The quasi-metallic behavior of highly doped conducting polymers cannot be explained by polaron hopping itself, therefore, also additional mechanisms at microstructure level need to be taken into account. Figure 5 D presents a schematic picture of microstructure of a disordered conducting polymer. Depending on the type of conducting polymer, method of synthesis and chain modifications, some parts of the polymer matrix can be organized into regions with high crystallinity. Crystalline regions with extended density of states are separated by vast disordered regions rich in localized states. In principle, charge carriers can propagate from one crystalline region to another through localized states near the Fermi level *via* resonance tunneling [17].

Summarizing, the charge transfer mechanism in organic semiconductors and particularly conducting polymers is of a complicated nature. Electrical conductivity is strictly dependent on charge carrier mobility and dopant concentration. In contrary to inorganic semiconductors the carrier mobilities are low and a high concentration of dopant is needed in order to achieve enhanced electrical conductivity. Propagation of charge carriers (*e.g.* polarons) in conducting polymers can be explained by several models which are based on variable range hopping. The proper understanding of charge transport mechanisms in conducting polymers is highly beneficial in designing organic electronic and chemical sensor devices.

2.2. Optical properties

Optical properties of materials strictly relate to electronic transitions upon excitation. The ground (S_0) and excited (S_n) states can be considered as potential wells within which the

energy levels are associated with the vibrational motion of molecules. Figure 6 A presents idealized potential energy curves and different vibrational energy levels for a diatomic molecule. Vibrational motions can be described using the concept of harmonic and anharmonic oscillator approximations. The potential energy of a harmonic oscillator depends on the force constant (f_c) related to thermodynamic binding energy and the distance between atoms or molecules. Since vibrational motions rely on the difference in the actual physical distance between molecules and equilibrium distance (R_e) with a non-zero vibrational energy (even for the lowest quantum vibrational number (v_0)). Anharmonic oscillator approximation characterizes deviation of potential energy from Hooks law (harmonic approach) and is dependent on dissociation energy which describes energy required to impart atoms in one molecule. When considering only the harmonic oscillator approximation, the vibrational energy levels can be represented by the following equation:

$$E_v = \frac{1}{2\pi} \sqrt{\frac{f_c}{m_r}} \left(v_n + \frac{1}{2} \right) \quad (2)$$

Where: E_v is energy in Hz, f_c is the force constant in N m^{-1} , m_r is the reduced mass ($m_r^{-1} = m_1^{-1} + m_2^{-1} + \dots$) in kg and v_n is the vibrational quantum numbers ($n = 0, 1, 2, \dots$). According to equation 2 the energy difference between each energy level with v_n is equal to the fundamental frequency. Spectral density of materials upon excitation is the sum of transitions from vibrational modes of ground to the excited states (Figure 6 B). The sharp peaks correspond to specific transitions which are symmetry allowed and the broad absorption or emission bands are an overlap of many specific transitions in the material. Absorbed energy from ground (S_0) to the first singlet excited state (S_1) can be released again and this photon emission is called fluorescence. For the systems having additional triplet states (different combination of spins than singlet state) the excited electrons from S_1 can be “trapped” in a triplet state which has a slightly lower energy. The transition from triplet to the ground state is called phosphorescence and is significantly slower than fluorescence. Stokes shift refers to the energy difference between positions of absorption and emission band maxima (*vide* Figure 6

B). This shift in energy is mainly connected with system relaxation, other structural reorganizations and arrangements can however also contribute to the shift.

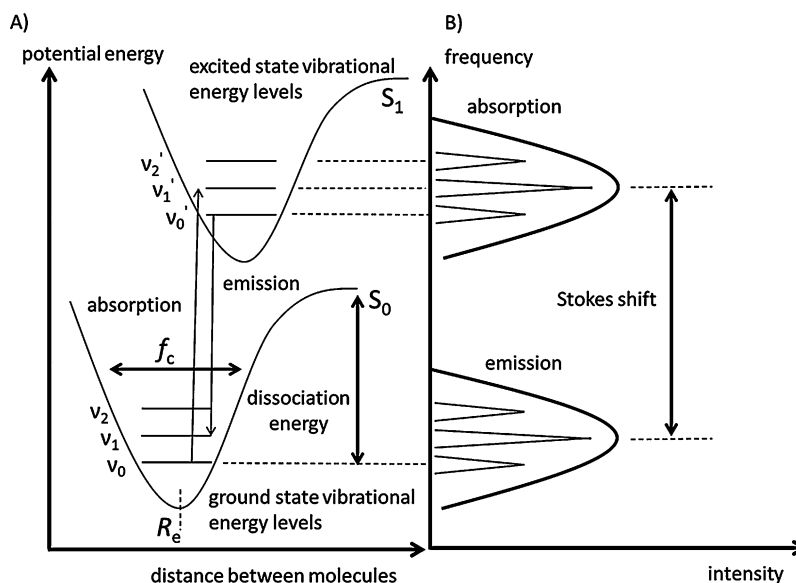


Figure 6. Idealized representation of the ground (S_0) and first excited (S_1) states of a diatomic molecule vs. potential energy (A). Corresponding optical absorption and fluorescence emission bands (B).

In conducting polymers photoexcitation of an electron from HOMO to LUMO level creates a singlet exciton. The formed intra-chain exciton is the analog of a polaron (Figure 4), however with positive and negative charge at the ends of the quinoid structure. The evidence for formation of self-localized excited states upon illumination (Figure 7 A) can be found from exciton binding energy studies and photoluminescence spectrum of poly(paraphenylenevinylene) (PPV) which is shifted (Stokes shift) with respect to the optical absorption spectrum [18,19]. Conducting polymers can be used in light-emitting diodes (LEDs) where the luminescence is created through radiative decay in a similar manner as photoluminescence [20]. As shown in Figure 7 B upon application of voltage, electrons from cathode site can be injected to the LUMO level of conducting polymer layer thus forming negatively charged polarons and analogously holes from anode site can be injected to the HOMO level generating positively charged polarons [20]. Both negatively and positively charged polarons combine into

a singlet exciton and the process of light emission is called electroluminescence. Importantly, quantum efficiency (the ratio of produced photons to injected charges) for electroluminescence is significantly smaller than for photoluminescence, due to a loss of 75 % of electron-hole pairs to triplet states [21]. The problem in efficiency of LEDs based on PPV have already been extensively studied and partly overcome by the use of copolymers or bilayer devices [22,23].

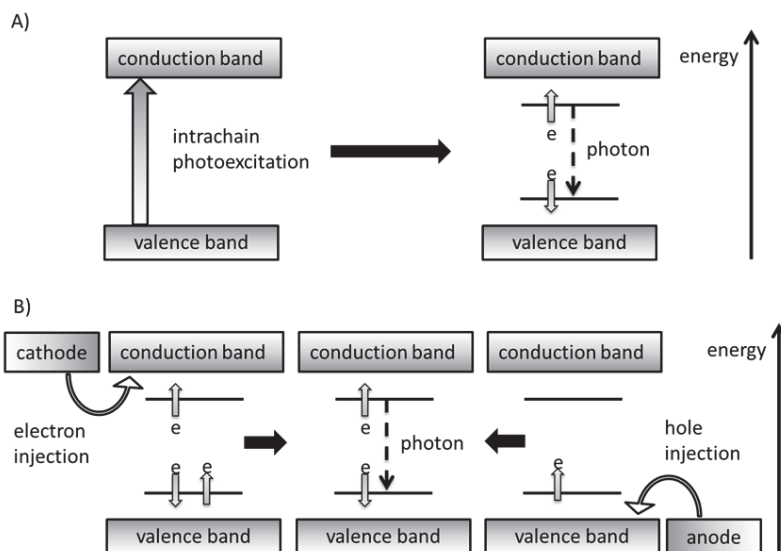


Figure 7. Idealized representation of photoluminescence (A) and electroluminescence (B) in conducting polymers for singlet excitation radiative decay.

2.3. Chemical and electrochemical synthesis

Chemical activity of any substance is a measure of the ability to undergo chemical reactions. Vast and extremely versatile chemical reactions can be involved in production of conducting polymers ranging from classical polymer and organic chemistry methods to electrochemical polymerization. Additionally, synthetic routes can be assisted with the use of different catalysts. Selection of a synthetic method depends on the desired application of the conducting polymer. For fundamental studies of conducting polymers and chemical sensors fabrication, electrochemical polymerization can be favorable due to its simplicity (one step synthesis) and a high control over the deposition process. Electrochemical synthesis involves

oxidation or reduction of the monomer species in electrolyte solutions to obtain usually compact films directly on the electrode. Although, electrochemical polymerization is useful in direct preparation of electroactive films, the major disadvantage of this approach is in insolubility of the product. From an industrial point of view it is important to study and develop conducting polymer inks that can be casted, spin coated or deposited on different substrates to fabricate electronic or sensor devices. Thus, for larger scale production chemical methods are preferable since they can provide solution processable conducting polymers either in their undoped or semi-conducting state.

Electrochemical synthesis can be performed by using different ways of application of the potential or current to the conducting substrate immersed in an electrolyte containing the starting monomer. The most simple electrochemical methods used in film preparation includes potentiostatic or galvanostatic (constant potential and constant current respectively) polymerization within a two- or three electrode system. If the growth of polymer and the occurring reactions are desired to be monitored then potentiodynamic methods (usually cyclic voltammetry) are used in a three electrode system. The three electrode set-up for electrosynthesis consists of a counter (control of current), a reference (control of potential) and a working (conducting substrate) electrode, usually abbreviated CE, RE and WE, respectively. The exact mechanism of oxidative polymerization is still unknown, however, it is assumed that during anodic oxidation of monomers radicals are formed which through radical-radical coupling merge into intermediate structures that further deprotonate to oligomers [24]. When oligomer chains reach a certain length they deposit on the working electrode due to loss in solubility [25]. Figure 8 presents an example of a possible mechanism of electrochemical polymerization of PPP starting from benzene *via* dimerization.

The formed electroactive film contains counterions (*i.e.* doping ions) incorporated from the solution and the resulting polymer film can be in different oxidation states depending on the procedure and method used. The reactions taking place in the vicinity and at the surface of the working electrode are depending on several parameters like: chemical activity of the starting monomer and its concentration, current density/electrodynamic conditions as well as the

physicochemical properties of salt and solvent used [26]. All common conducting polymers listed in Figure 1, can be prepared electrochemically excluding trans-PA [24,27-29]. This archetypical conducting polymer can be prepared chemically from acetylene *via* ring opening reaction in the presence of metathesis catalyst [30]. Also, polymers which are complicated in structure like *e.g.* ladder-type systems and based on copolymers need to be prepared *via* chemical methods [30,31]. Importantly, oxidative polymerization of conducting polymers can be performed by chemical synthesis using oxidizing agents. So the synthesis of PPy can *e.g.* be assisted with $\text{Fe}(\text{ClO}_4)_3$ and PEDOT or its derivatives with FeCl_3 oxidants, respectively [33-35]. Highly solution processible PEDOT doped with poly(styrenesulfonate) (PSS) surfactant is produced in large-scale. The synthesis of commercially available PEDOT:PSS is usually made in PSS electrolyte using $\text{Na}_2\text{S}_2\text{O}_8$ as the oxidizing agent [36].

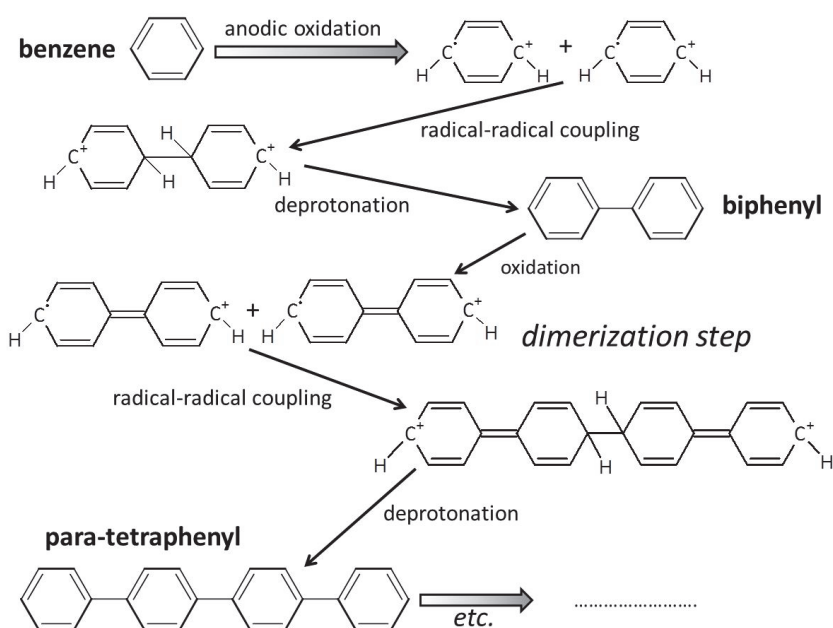


Figure 8. Schematic representation of electrochemical polymerization of PPP starting from benzene.

3. Selected applications of conducting polymers

3.1. Organic electronics

Conducting polymers and other organic semiconductors have been already intensively studied for electronic materials. The major research is focused to fabricate organic LED (OLED), field-effect transistor (OFET) and solar cell (OSC) devices, opening the “era of plastic electronics”. Organic electronic devices are usually manufactured in thin-layer technology (micro- and nanometer scale) by different printing methods utilizing solution processable materials. Hence, conducting polymer based devices can outdistance “traditional” inorganic technology in mechanical flexibility, weight and cost to performance ratio.

In the basic form, OLED devices consist of an emissive layer sandwiched between two electrodes and upon application of electricity light is generated (electroluminescence). The operating principle of OLEDs can be seen in Figure 7 B. The reason for the great scope on OLEDs is that they can be used for display manufacturing providing thinner, more efficient and less power consuming displays than conventional LED or liquid-crystal technology [37]. In fabrication of OLED devices, conducting polymers can be used either as an anode or emissive material or both simultaneously. Among conducting polymers and their derivatives that are used for an emissive layer are PPVs, PPPs, polythiophenes (PTs) and polyfluorens (PFs) [38-41]. For application of OLEDs in real displays the important is the proper generation of three basic colors (red, green and blue) in order to generate the desired color. PPVs and PFs have been found to provide tunable emission frequencies and relatively high quantum yields. The emission colors of those polymers span the visible spectrum, however, it was found that PPV-based materials are useful as red and green OLEDs and PFs complement with efficient emission of blue color [42]. A typical anode material for LED devices is indium-tin-oxide (ITO) glass despite its very high surface roughness which causes adhesion problems to organic layers not desired for flexible electronics [43]. Therefore, there were attempts to exchange ITO with thin and transparent layers of PEDOT:PSS. Application of this conducting polymer greatly improves external quantum efficiency and mechanical stability with respect to devices with ITO as the

anode material [44]. The major drawback of PEDOT:PSS is its relatively low work function, which however, can electrochemically be adjusted [45].

Another successful use of conducting polymers in organic electronic devices is in OFETs, particularly in organic thin-film transistor (OTFT) devices. Usually an OTFT device consists of electrical conductors named "source" and "drain" deposited on insulator layer and separated by a semiconductor. The device is complemented by an additional conducting layer termed "gate" which is in contact with the insulator. When the voltage is applied between the source and the gate electrodes current is passing through the semiconductor from source to drain. Hence, the conductivity is a function of the applied potential. The important parameters of transistors are ON/OFF ratio and the value of potential needed to induce current flow in the semiconducting channel. Solution processable organic materials can be used in OTFTs, reducing the manufacturing cost, providing lower operation voltages and better flexibility in comparison to inorganic-based TFTs [46]. The major drawback of OTFT devices is the relatively low carrier mobilities, affecting the ON/OFF ratio, hence, traditional TFTs will still be used in applications requiring very high switching speeds [46]. Conducting polymers are used in OTFT devices either as the semiconductor layer or the electrode material. Frequently used solution processable polymers in fabricating the semiconducting channel in FETs are PTs and PPVs derivatives [47-49]. Importantly, ambipolar transistors (both p- and n-type semiconduction possible in one device) have been realized by using blends of PPV derivative with functionalized fullerene or ladder-type conducting polymer mixed with copper phthalocyanine dye [50,51]. PEDOT:PSS and PANI conducting polymers can be used for organic source and drain electrodes, yielding an excellent alternative to the costly metal conductors, especially if those polymers are exposed to secondary dopants [52,53]. Also, PEDOT:PSS was used to fabricate an electrochemical transistor where PEDOT:PSS was employed both as the active switching and source/drain layers [54].

In principle, a solar cell works as a converter of light into electricity. The whole concept of OSC devices is to some extent an inverted process found in electroluminescent devices (*vide* Figure 7 B). OSCs are usually made of thin layers of donor and acceptor materials. Incident photons

are absorbed by the donor material and the π -electrons from HOMO level “jump” to LUMO level, thus excitons are created which diffuse to the donor/acceptor interface and dissociate into charge carriers. When an exciton reaches this interface the induced electron from LUMO of donor is then transferred to the LUMO of acceptor layer. Hence, the charge can be transported to the electrode (*e.g.* aluminum) generating electricity. The major reason for the great scope of development of OSCs is the reduction of production costs with respect to silicon-based solar cells which require manufacturing in vacuum. In order to practically realize competitive OSC devices, materials with efficient absorption of light, charge transfer and separation are needed [55]. The best in overall power conversion efficiency ($\sim 11\%$) OSC so far, is the so-called dye sensitized solar cell (DSC) in which adsorbed porphyrin dye on crystalline TiO_2 particles absorbs light and electrons are injected into the conduction band of TiO_2 particles [56]. In DSC the positive charge is transported by the liquid electrolyte to the counter electrode, which makes this approach not suitable for many industrial applications. Since conducting polymers are stable against photodegradation in an inert atmosphere and their optical band gap can be tuned to match properly the visible spectrum, they have been utilized as donor layer in heterojunction devices or directly blended with fullerene-based electron acceptor materials [57,58,59]. The use of PT derivatives as donor material in composite devices yielded up to 5 % of power conversion efficiencies which is a significant achievement in comparison to bilayer devices [60]. However, in order to commercialize OSCs based on conducting polymer composites the energy loss in the electron transfer from donor to acceptor material has to be minimized together with proper matching of the polymer band gap [61].

3.2. Chemical sensors and biosensors

Recognition of chemical substances and their concentrations in confined systems is provided by sensing devices based on specific analog signals. Electrochemical sensor devices convert “chemical information” into electronic signal (*i.e.* transduction) that can further be processed and interpreted in terms of a scientific model (Figure 9 A). Depending on the measured electrical quantity, electrochemical sensors can be divided into: potentiometric, amperometric

and conductometric sensing groups where the respective change in electrical potential (E), current (I) and conductance (G) accounts for the recognition process. An electrochemical sensor device can be seen as an electrical circuit where specific chemical phenomena having mixed resistive and capacitive behavior, are part of this circuit. Thus, the change in electrical quantities within a circuit relates to the presence of *e.g.* ions in a solution. In order to get precise information on concentration of the analytes, this relation needs to be described by a linear or logarithmic function. Hence, the detection limit of electrochemical sensor is confined to the extension of linear range. A generalized description on a three electrode system of electrochemical measurement is shown in Figure 9 B.

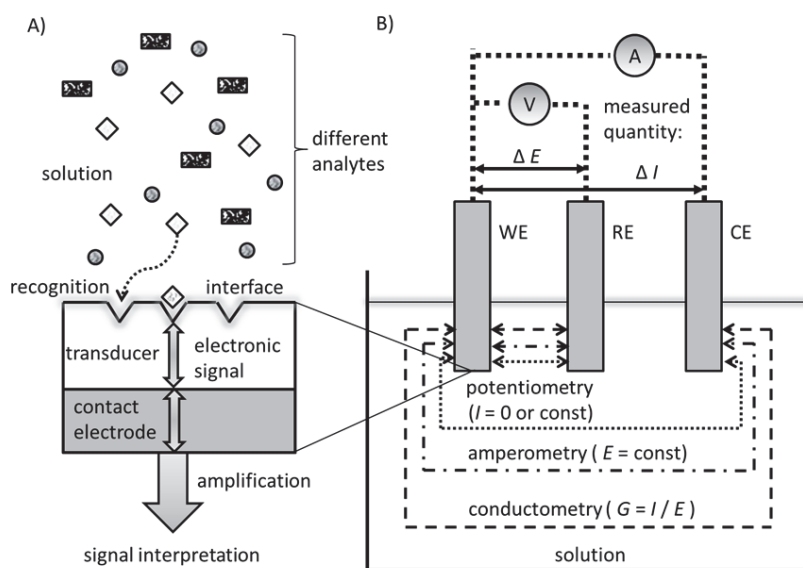


Figure 9. Generalized and simplified representation of the transduction process (A) and detection methods (B) specific for electrochemical sensors.

However, practical potentiometric detection of ions is based on a two electrode system under zero current condition where the electromotive force (*emf*) is measured between WE and RE. Zero current potentiometry is utilized in the so-called ion-selective electrodes (ISE) where mono- or multivalent ions can be quantitatively analyzed using ion-selective membranes (ISM) containing compounds for selective binding of ions. On the other hand, non-zero current potentiometry (*i.e.* chronopotentiometry) where the current is kept at a constant level for a

certain time polarizing the WE (*e.g.* ISE) is performed within a three electrode system. For amperometric detection the potential is constant within measurement time and an overall output signal is determined (ideally) by mass-transport resistance attributed to analyzed sample. Conductometric sensors, also referred to as chemiresistors are usually used for recognition of gases or biological species. In this group of sensors the analytical information is obtained due to the change in resistivity of a selective material. All electrochemical sensing groups listed in Figure 9 B can greatly benefit from the use of conducting polymers as a transducer layer, mostly due to the possibility to enhance the rate of redox processes, relatively easy immobilization of selective molecules, flexibility in sensor design and biocompatibility. Importantly, by using conducting polymers in the sensor structure various electrochemical sensors can be miniaturized and fabricated at low cost. Subjectively the most notable enhancement of the recognition process with the use of conducting polymers was carried out within amperometric biosensors and ISEs.

In the amperometric sensors, the measured current is proportional to the concentration of the analyte and therefore the systems used in recognition should be easy to be oxidized and reduced. Owing to the fact that products of enzymatic reactions *e.g.* O₂ or H₂O₂ can be accurately detected [62,63], amperometric sensors have extensively been used as biosensors. The first application of conducting polymer for entrapping an enzyme emerged already in 1980s [64]. In this approach, PPy was electrosynthesized in the presence of glucose oxidase showing the feasibility of manufacturing robust amperometric glucose sensors. Since then, several enzymes have been immobilized for detection of many important biologically active compounds, mostly in *e.g.* PPy [65-67], its methyl derivative [68], PANI [69,70] and PEDOT [71]. Also, macromolecules like deoxyribonucleic acid (DNA) can be amperometrically detected on PPy films modified with immobilized or absorbed oligonucleotide fragments [72-74]. Amperometric detection of DNA assisted with conducting polymers appealed an extensive attention, together with immobilization of antibodies into conducting polymer matrix to create immunoassays. The latter, resulted in immunosensors that can be fabricated at low cost and also importantly with direct detection of the target species [75,76].

In ISEs, conducting polymers are mainly used as ion-to-electron transducers. This approach enables the possibility of miniaturization of the device and also greatly simplified the manufacturing process in comparison to classical ISEs where an inner reference solution is always needed. The so called all-solid-state ISE typically consists of either an electropolymerized or solution casted conducting polymer layer with an ISM deposited on top. In such a design the overall enhanced ion recognition (especially toward lowering of detection limit) is attributed to synergy of the interfacial redox properties of the conducting polymers [77] and the high selectivity of ISM [78]. There are numerous examples of conducting polymers used as transducer layer in solid-state ISEs for the detection of ions that are important for medical or environmental analysis [79]. For instance selective detection of K^+ was realized by using PPy, PEDOT or PANI [80-82] and nanomolar detection of Pb^{2+} was accomplished by utilizing PPy [77]. The other promising approach for selective potentiometric detection of ions is in a direct use of conducting polymer both as the transducer and the selective layer. This concept might provide miniaturization of ISEs to nearly a nanodomain and possibility for immobilizing biomolecules within a single-layer. Conducting polymer single-layer ISEs were already extensively studied for detection of cations or anions (*e.g.* pH, Ca^{2+} , Cl^-). However, they are still limited in their overall performance in comparison to sensors with ISMs [79]. Another highly important application of conducting polymers in zero-current potentiometry is fabrication of liquid-junction free RE. In order to practically realize integrated chemical sensor the RE needs to also be miniaturized. Notable examples in development of liquid-junction free REs are utilization of conducting polymers doped with pH buffering ligands [83] and a systematic study on surfactant doped PEDOT and PPy covered with poly(vinyl chloride) (PVC) based membranes [84].

4. New monomers and electrolytes for electrochemical synthesis of electroactive materials

4.1. Polycyclic aromatic hydrocarbons

Fused aromatic molecules have attracted attention as building blocks of polymer backbone mostly due to the possibility of synthesizing new fluorescent materials. *E.g.* compounds such as anthracene and pyrene were used as monomers to make conjugated polymers or copolymers

[85,86]. Those molecules belong to a wide group of compounds termed polycyclic aromatic hydrocarbons (PAHs) which are polycyclic organic molecules consisting only of fused rings and exhibiting a high degree of aromaticity [87]. There is a huge variety of PAHs in both sizes and symmetries, ranging from naphthalene (bicyclic aromatic hydrocarbon) to macromolecules consisting of more than two hundred fused rings [88]. Since PAHs in different arrangements are formed during incomplete combustion of organic compounds they are widely spread through the terrestrial environment [89]. Owing to the usually planar, aromatic and plain structure of PAHs, those molecules have a relatively high π -electron overlap and characteristic optical spectra. Selected PAHs of environmental, astrophysical and materials science interest are listed in Figure 10 A. The reason for the numerous publications concerning PAHs are mainly related to the cancerogenicity of relatively small PAHs (especially BaP) [90] and the formal similarity of larger PAH molecules to both graphene and disordered graphite [91]. Interestingly, vibrational motions of PAHs in different sizes and symmetries are being attributed to characteristic undefined vibrations in the emission spectra of interstellar medium [92].

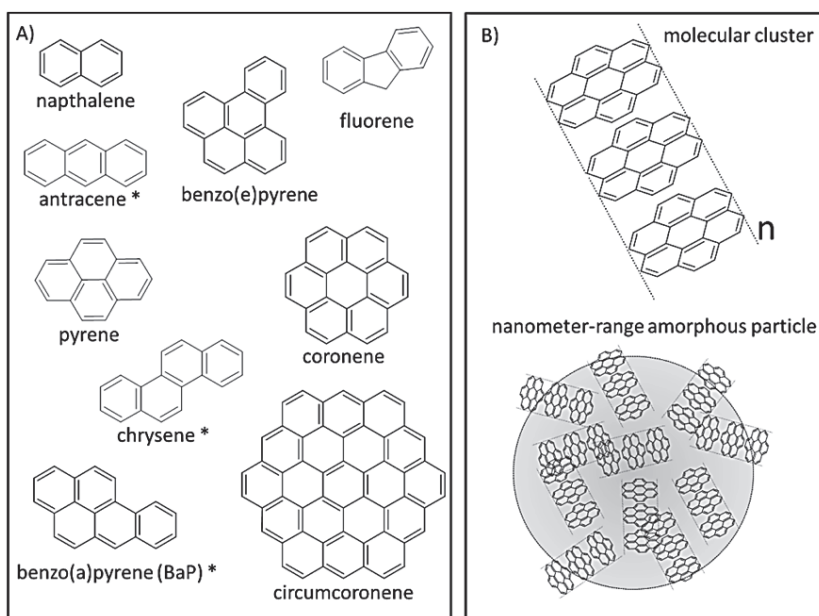


Figure 10. Chemical structures of PAHs selected as an example (A) together with a schematic representation of π -stacking of PAHs molecules and formation of particulate matter made of randomly distributed PAH clusters (B).

As already mentioned, some of the PAHs have been used to synthesize conducting polymers. Vast majority of the methods to synthesize PAHs-based copolymers, linear chains or functionalized conducting polymers rely on chemical synthesis [85,86,93]. However, also electrochemical synthesis can be successfully used in fabrication of polypyrrole and its copolymers [94]. Another concept in application of PAHs molecules in organic electronics is in the alignment-controlled deposition of planar PAHs. In nature, owing to the interactions of delocalized π -electrons between planar molecules, PAHs tend to form molecular clusters as shown in Figure 10 B. With the growth of a cluster the overall energy of the PAH based molecular system is minimized and this extension is limited to certain length governed by particular physical conditions. Therefore, PAH clusters aggregate to form amorphous particles which can be found *e.g.* in particulate matter resulting from incomplete combustion of hydrocarbons [95]. In order to take advantage of spontaneous formation of PAH clusters, numerous publications are devoted to functionalize PAH molecules with aliphatic chains in order to make them solution processable [88]. Derivatized PAHs self-assemble to form so-called discotic liquid crystals which are highly ordered structures with anisotropic properties [88,96]. On the other hand, non-ordered PAH aggregates could also be beneficial *e.g.* in electroactive templates for sensor or in electrocatalytic applications. The major benefits of synthesizing such template materials resides on enhanced ion-to-electron transduction in comparison to conducting polymers and affinity of PAHs to carbon-based substrate electrodes minimizing charge-transfer resistance at the WE/conducting layer interface.

4.2. Room temperature ionic liquids

In order to enable any investigations of chemical phenomena and processes taking place at electrified interfaces, the medium in which ions or compounds of interest are dissolved need to exhibit sufficient ionic conductivity. This is practically realized through salt, acid or base additives (*i.e.* electrolytes) which are selected for particular applications. For electrochemical synthesis and doping studies of conducting polymers in non-aqueous media the most common electrolyte is salt solution. There is also a substantially different class of electrolytes that act both as solvents and ionic conductors at the same time. These potentially useful media are in

principle salts in molten state and are usually referred to as ionic liquids. Since the liquid range of salts obviously depends on their melting points and thermodynamic stability, it was practically adopted that an ionic liquid is a salt that melts below ~ 100 °C. This nomenclature distinction is arbitrary, and therefore in this work any molten salt which is in liquid state at ~ 25 °C is referred to as room temperature ionic liquid (RTIL).

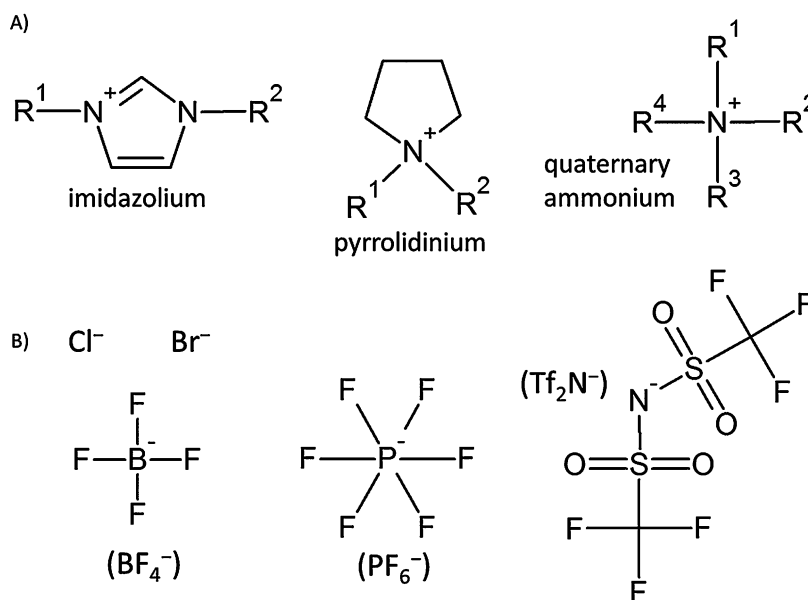


Figure 11. Chemical structures of some most common cations (A) and anions (B) constituting RTILs. Note: numbered side groups (R^n) refer to different alkyl substitutes and Tf_2N^- stands for bis(trifluoromethylsulfonyl) imide.

The reason that RTILs remain liquid at ambient temperatures is attributed to a significant difference in size between anions and cations with relatively low symmetry which prevents packing of the lattice [97], as well as charge dissipation [98] and steric hindrance effects [99]. Therefore, representative RTILs consist of bulky organic cations and inorganic anions some of them illustrated in Figures 11 A and B. From the applied electrochemistry point of view RTILs exhibit potentially useful properties such as: relatively high ionic conductivity and viscosity, almost negligible vapor pressure, and a wide electrochemical window (*i.e.* redox-free potential range) [100,101]. Thus, RTILs have been used as media for electropolymerization and doping studies of conducting polymers greatly enhancing in some cases the deposition process and

electrochemical activity of the resultant films in comparison of what can be achieved with conventional electrolytes. Additionally, since organic solvents are highly volatile and toxic, RTILs can be considered as powerful alternative electrolytes. On the other hand the commonly accepted claim that RTILs are non-toxic solvents is not always valid [102]. Special concern need to be emphasized on the moisture-sensitivity of RTILs, since the products of uncontrollable reactions of *e.g.* chloroaluminate anions or PF_6^- with water, can lead to the formation of highly corrosive acidic environments [103,104]. Also, even for the hydrophobic and moisture-stable RTILs, the water content for some particular applications needs to be precisely controlled, due to a drastic decrease in the available electrochemical window with increasing amount of water [105].

Moisture-stable RTILs have successfully been used as electrolytes for electrochemical polymerization of *e.g.* PANI [106], PEDOT [107,108], PPy [109,110] and PTs [111]. The observed pronounced enhancement in quality (*e.g.* decreased surface roughness), electrochemical activity or thickness of the resultant conducting polymer films can be attributed to particular properties of the studied RTILs. Since polymer growth is dependent on concentration of the reaction products in the vicinity of the electrode, relatively high viscosities of RTILs facilitates limited transport of those products away from the solution/electrode interface [109]. Also, the amount of incorporated ions during electrosynthesis is higher in RTILs in comparison to conventional electrolytes based on molecular solvents [110], which hypothetically results in both enhanced electrochemical activity and quality of polymer films. Moreover, due to the extended electrochemical window of RTILs, it is possible to dope conducting polymers at extreme potential levels. Application of RTILs in electrochemical synthesis of conducting polymers could be beneficial in fabrication of *e.g.* amperometric or potentiometric sensors with considerably higher electrical conductivities facilitating enhanced transduction.

5. Synthesis, characterization and deposition techniques of studied electroactive films

5.1. Cyclic voltammetry

In this work cyclic voltammetry (CV) was extensively used as a major technique for electrochemical synthesis and doping studies of conducting polymers and other electroactive materials. This potentiodynamic method was also combined with vibrational spectroscopy and chemiresistive studies to provide additional information about changes in electronic structure and conductance during redox reactions. In CV the voltage is swept at fixed rate between two values, one below (E_1) and one above (E_2) the formal redox potential ($E^{\circ'}$) of the analyte. Hence, within one linear potential scan from E_1 to E_2 , oxidation of the analyte occurs. The oxidized form of the analyte is reduced back to its original form during the reverse scan.

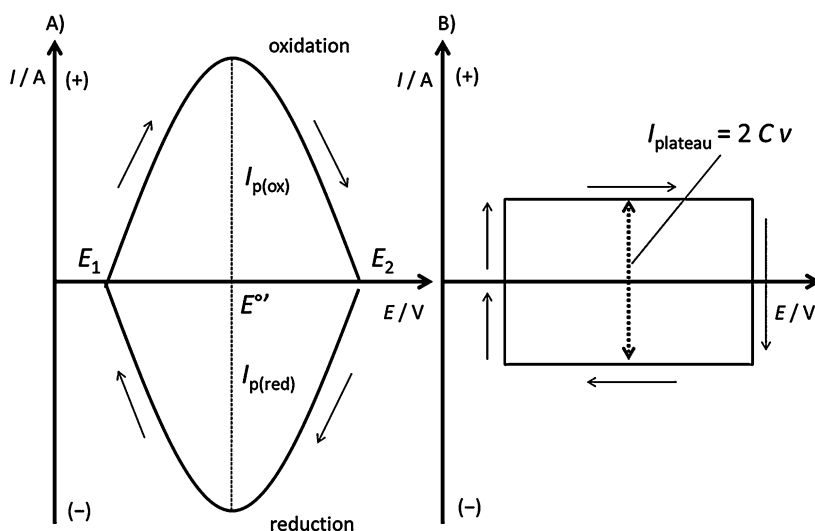


Figure 12. Idealized cyclic voltammograms for a reversible reduction of a hypothetical redox couple attached to the electrode surface (A) and a system corresponding to a pure capacitor without any redox reactions present (B). Note: arrows represent “direction” of polarization of the WE.

Redox reactions are normally studied in a three electrode system as already schematically shown in Figure 9 B. For practical assay work, the recorded current during potential cycling is plotted against the applied voltage resulting in the so-called cyclic voltammogram. A highly

idealized current-voltage curve of a hypothetical redox couple reversibly reduced at a macroelectrode surface is shown in Figure 12 A. Shape of the cyclic voltammogram is dependent on the potential scan rate, electrode geometry, concentration of the oxidized/reduced species and number of electrons involved in the process. Additionally, for real systems, the diffusion coefficient of electroactive species strongly influences the shape of the cyclic voltammograms. At macroscale the change in concentration with time is non-zero, thus steady-state current conditions are not reached, leading to the formation of characteristic peaks in the cyclic voltammogram. The height of those peaks can be described by the Randles-Sevcik equation:

$$I_p = k_s n_e^{3/2} A D^{1/2} \nu^{1/2} c_b \quad (3)$$

Where: I_p is the peak current in A, $k_s = 269000$, n_e is the number of transferred electrons, A is the surface area of the WE in cm^2 , D is diffusion coefficient in $\text{cm}^2 \text{s}^{-1}$, ν is scan rate in V s^{-1} and c_b is the bulk concentration of the electroactive species in mol cm^{-3} . Note: equation 3 is valid assuming that the system is near room temperature. What is practically important in equation 3 is the direct proportionality of the peak current (I_p) to both c and $\nu^{1/2}$. Therefore, CV can be used for detection/monitoring of electroactive species and simultaneously study kinetics of the reaction. Moreover, the number, shape, presence or absence and position of some particular peaks in the cyclic voltammogram can give useful information about *e.g.* reversibility/irreversibility, oxidation states, reaction mechanism, adsorption or deposition process. Additionally, the surface area under any current-voltage curve is in principle the charge (Q) which passed during the electrochemical process. Therefore, the capacitance ($C = Q / V$) involved in those processes can apparently be calculated. Figure 12 B presents the cyclic voltammogram of an ideal capacitor implying the “plateau current” which is directly proportional to the scan rate. Conducting polymers with dominant capacitive behavior yield cyclic voltammograms with rather similar features. In real CV studies of *e.g.* conducting polymers, the resulting current-voltage curves are a combination of several redox reactions, capacitance of the polymer film and WE as well as a bulk physicochemical properties of

electrolyte. Therefore, in order to assign the obtained energy dispersion to a specific system, knowledge about the background or interfering currents is needed. In conclusions, CV can relatively easily be implemented in analytical methodology providing practically useful electrochemical information.

5.2. Molecular spectroscopy

Electronic and molecular structures of different materials characterized in this work were investigated using both *in situ* attenuated total reflectance-Fourier transform infrared (ATR-FTIR) and ultraviolet-visible light (UV-vis) spectroscopies. Information about molecular structures was obtained by Raman spectroscopy. The ATR-FTIR spectra were recorded simultaneously with CV and for *in situ* UV-vis spectroscopy different constant potentials were applied.

In optical spectroscopy, analytical information is obtained from the changes in the intensity of the transmitted light during a frequency scan over different excitation wavelengths (Figure 13 A). The IR spectra considered in this work ranges from ~1250 to 16000 nm covering the so-called infrared active vibrations (IRAV) specific for each chemical compound and the electronic absorption region which rises upon the applied electric field to a semiconductor. Within the UV-vis part of the electromagnetic spectrum the fundamental transition denoted as either $\pi^* \leftarrow \pi$ or $S_1 \leftarrow S_0$ (*vide* Figure 3 A and Figure 6 A, respectively) occurs. Since in IR spectroscopy the absorbed energy is considerably lower than in UV-vis, the molecular vibrations give rise to the observed vibrational modes corresponding to stretching and bending modes of the studied molecules. The energy of those modes can sufficiently be described with harmonic oscillator approximation shown in equation 2. What is practically measured in IR spectroscopy is the change in molecular dipole moment during the vibration. Figure 13 B shows the principles of any spectrometer. Macroscopically the intensity of photons interacting with molecules decreases exponentially according to Lambert-Beer law. The attenuation coefficient (γ_f) is specific for each type of material and the used excitation wavelength. Hence, both FTIR and

UV-vis spectroscopies can be used for quantitative analysis within the linear dependence between absorption and concentration of the analyte.

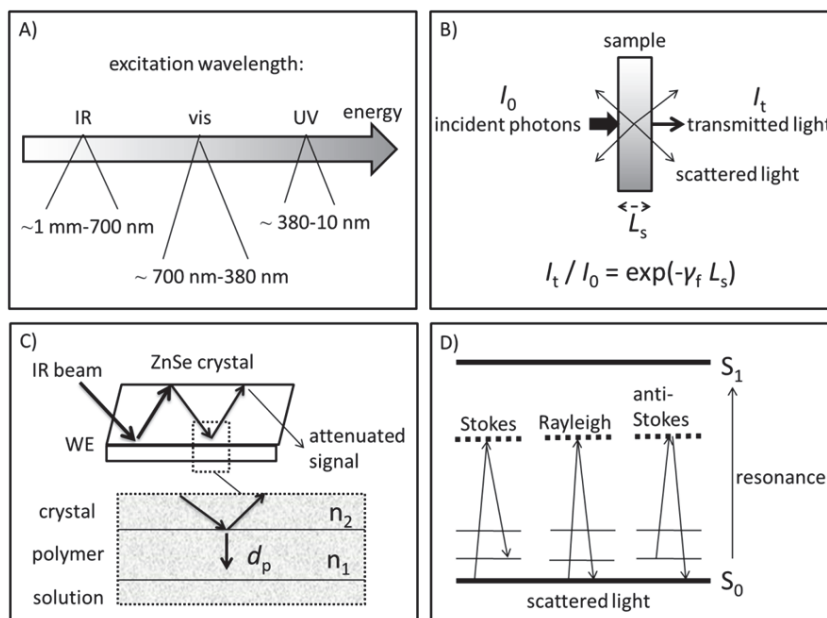


Figure 13. The part of the electromagnetic spectrum specific for absorption spectroscopy (A). Schematic representation of the types of detection in a spectrometer (B). The principles of the *in situ* ATR-FTIR measurement [112] (C). Jablonski diagram showing Raman effect (*i.e.* Stokes and anti-Stokes scattering) together with resonance Raman transition and elastic Rayleigh scattering (D).

Depending on the measured physical quantity, vibrational spectroscopy can be divided into the already discussed IR and analytical methods based on the so-called Raman effect. As shown in Figure 13 B part of the light is scattered from the sample. Scattering of the visible light is actuated by induced vibrating dipole moments of the molecules which are dependent on the changes in the polarizability of the molecule. Three distinct scattering processes (Figure 13 D) are involved, each of them with different frequencies governed by the Boltzmann distribution. The dominant process is the elastic interaction referred to as Rayleigh scattering followed by the so-called in-elastic Stokes and anti-Stokes scattering. Practically in Raman spectroscopy only the in-elastic Stokes scattering is used for determination of molecular vibrations. Incident photons with energy lower than the electronic excited state would elevate electrons to virtual

levels and then the system is relaxed to specific vibrational levels in the electronic ground state. Therefore, IR and Raman are complementary methods, each providing essentially the same information about vibrational levels, and depending on changes in dipole moment or polarizability of the vibrating molecules, the vibrations are only IR or Raman active or both.

In modern spectrometers IR spectral data are collected over a wide frequency range using Michelson interferometer. The resultant interferogram (*i.e.* the function of relative intensity and the position of beam-splitting mirrors) is mathematically transformed into the IR spectrum by fast Fourier function. FTIR spectra can be also recorded when the IR beam passes through *e.g.* a ZeSe, Ge or diamond crystal specifically fabricated to obtain total internal reflection. Total reflection is obtained when propagating light encounters a medium with different refractive index (relation of the light velocities in vacuum and the optical medium) at a certain angle. In principle, the reflected wave is attenuated due to the evanescent effect. Always, some fraction of light penetrates the boundary between the crystal and the other optical medium. For the system presented in Figure 13 C, the penetration depth (d_p) depends on the wavelength of the used radiation, the ratio between the two refractive indexes (n_2/n_1) and the angle of incidence. Since the value of d_p can be even in the micrometer range, ATR is a powerful tool in studying the optical properties of thin polymer films.

In a typical *in situ* ATR-FTIR measurement, a thin layer of platinum is sputtered on one side of the ZeSe crystal [112]. Hence, a WE is created on which the conducting polymer can either be grown or drop-casted. The whole crystal can be assembled into a three-electrode system cell. Therefore, this “combined” technique can be used to study changes in the IR spectrum which are induced by increasing the magnitude of the electric field. Upon doping of semiconductors the created charge carriers and their concentration have an influence on the symmetry of the molecule, and also on the number of vibrational transitions. Thus, the relative intensity of the IRAV bands is increased and their position in the spectrum could change drastically. Moreover, since polarons and bipolarons are quasi-particles consisting of moving electrons or holes with surrounding deformation, the electrochemical doping induces rise of the electronic transitions associated with absorption as shown in Figure 6 A. The electronic absorption region is

dominated by significantly wide intense bands at energies higher than the IRAV bands. Information of the strictly electronic transitions were obtained by *in situ* UV-vis spectroscopy where the glass covered by a thin and transparent layer was coated by electroactive films and assembled in the three-electrode system cell. Doping was achieved by application of constant potential for a certain time, in contrary to *in situ* ATR-FTIR measurements where potentiodynamic measurements were used. These two spectroelectrochemical techniques are complementary yielding information about the molecular and electronic structures.

5.3. Electrochemical impedance spectroscopy

Since electrical circuits can be used as an approximation of real electrochemical systems, impedance spectroscopy have been utilized for determination of ion transport dynamics and electrical quantities associated with studied electroactive films. This technique, often referred to as electrochemical impedance spectroscopy (EIS), is in principle based on the measurement of the impeded (*i.e.* delayed) electrons passing through an examined system under applied electric field at different frequencies. Ideally, the flow of electrons in a galvanic cell is constant over time and the frequency is zero. Such a simple system can be expressed as a direct current (DC) circuit. However, the measured total opposition to electric current of many physical systems is dependent on frequency and therefore the Ohms law needs to be expressed as the following equation:

$$Z = |Z|e^{-j\Delta\theta} \quad (4)$$

Where: Z is the electrical impedance in Ω , j is the imaginary number equal to $(-1)^{1/2}$ and $|Z|$ is the modulus of the applied voltage divided by current related to measured phase shift ($\Delta\theta$) which is defined as a difference between voltage and current phase. The vector sum of current and voltage yields the value of impedance as shown in Figure 14 A. Hence, as can be seen from equation 4, the determined impedance in alternating current (AC) circuits is a complex number consisting of a real (Z') and an imaginary (Z'') component which can be related physically to in-phase resistance and out-of-phase capacitance respectively. Theoretically, if only the real part

of the impedance exist then the examined system exhibits pure resistor behavior (impedance independent of frequency). In contrary, if the flow of electrons is directly proportional to the rate of change of voltage with a $\Delta\theta$ equal to 90° , then only the imaginary part of the impedance exists yielding pure capacitor behavior. Moreover, if the frequency in an AC circuit is zero the impedance of a pure capacitor becomes infinite.

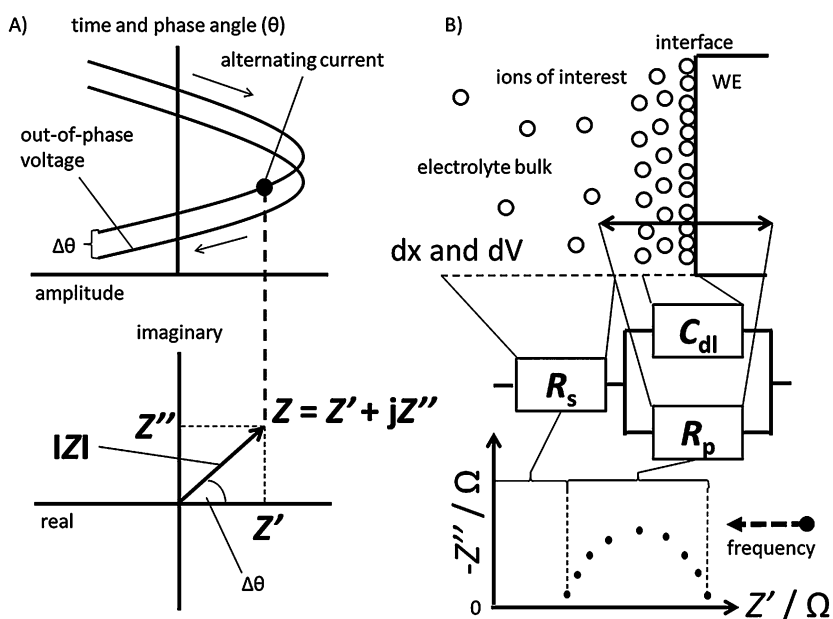


Figure 14. Representation of a sinusoidal-like time-dependent function of current and voltage shown as a vector product in a complex plane (A). Idealized charging process during polarization of WE limited by mass transport dynamics shown as a picture (top), equivalent circuit (middle) and Nyquist plot (undermost) (B).

Importantly, electrochemical systems can be expressed by series and parallel configurations of resistors and capacitors. Figure 14 B presents a mathematical description of a basic electrochemical phenomenon; the formation of the electrical double layer at the interface between WE and solution. Polarization of the WE results in the movement of charge carriers to the vicinity of the electrode and in capacitive charging of its surface. Since this process is influenced by a mass transport resistance, an overall determined admittance (an inverse of impedance in S) can be expressed by the following equation:

$$Y(\omega) = \frac{1}{R_s} + \frac{1}{R_p} (1 + j\omega C_{dl}) \quad (5)$$

Where: R_s and R_p are the solution and polarization resistance in Ω , respectively. The parameter ω is an angular frequency in rad s^{-1} and C_{dl} is the double layer capacitance in F. The value of R_s manifests in a complex impedance plane (also called Nyquist plot) as a shift of the “first” highest frequency from zero Ω and the value of R_p as a total diameter of the semicircle in the real part of the impedance. Equation 5 can be used as a practical model for many reactions which involve charge transfer and are not diffusion-controlled. The time constant of the parallel RC circuit can be associated with the kinetics of the studied reactions.

The relatively simple and intuitive model presented by equation 5 is useful in analysis of frequency dispersion graphs, since if the examined system gives only a semicircle in the Nyquist plot then one can directly draw conclusions about the electrical quantities of interest without any need of fitting procedures. On the other hand, for many electrochemical systems, the overall impedance within both frequency and energy (different oxidation/reduction levels) dispersion needs to be described by a non-intuitive model of imperfect capacitor, the so-called constant phase element (CPE). This versatile electrical element is nowadays widely used in equivalent circuit analysis in EIS [113]. CPE can model semi-infinite linear diffusion (special case of CPE referred as Warburg impedance) as well as pure resistor and capacitor. When CPE is in parallel with a resistor it can describe double layer capacitance and charge transfer involved in the polarization process. The major reason of the great success of CPE in modeling of many electrochemical systems relies on its ability to provide a robust approximation of porosity. The Warburg element is implemented in many equivalent circuits to describe diffusion. However, for thin and porous films it can yield unreasonable results. In such cases, hyperbolic functions can be applied providing information about finite-length diffusion. There are two “bounded Warburg” elements which are based on a cotangent hyperbolic function (referred as O element) and a tangent hyperbolic one (referred as T element) each describing the impedance of finite-length diffusion with a transmissive and reflective boundary, respectively.

The detailed analysis of frequency dispersion graphs is typically handled with fitting programs [113], since many of the elements in equivalent circuits can have very similar mathematical descriptions or their time constants can be close together. Considering the variety of models which can have physical meaning and fitting algorithms available, the EIS technique is indeed a powerful tool in modeling of *e.g.* electrochemical processes involved in chemical sensing. Moreover, redox reactions and capacitive charging of conducting polymers or other electroactive materials can be studied in detail, since impedance can be recorded at any constant potential of interest, providing information about energy dispersion in the examined systems.

5.4. Electrical conductivity and in-situ conductance measurements

Conductivity of the drop-casted conducting polymer films was determined in this work by using the four-point probe measurements. In this technique, the four probes (placed vertically in line on top of the sample) are equidistant and between the inner ones the voltage is recorded which corresponds to the applied constant bias current between the outer probes. Therefore, it is possible to exclude the spreading resistance which becomes significant in low resistive samples when two-point probes are used. From the four-point probe measurement the bulk resistivity can be estimated according to the following equation:

$$\rho = \frac{\pi}{\ln 2} L_f \left(\frac{E}{I} \right) \quad (6)$$

Where herein: ρ is the resistivity in Ω cm and L_f is the film thickness in cm. If L_f is excluded from above equation one gets information just about the so-called “sheet” resistivity. Depending on the application both resistivity values could be useful (*e.g.* for relatively very thin films the approximation of sheet resistivity alone L_f would be sufficient). Equation 6 is valid if L_f is smaller than half the probe spacing. Typically the conductivity of the samples is calculated using finite-size corrections with respect to L_f as well as to the size and shape of the film [114].

The four-point probe technique is practically useful to estimate the bulk or sheet resistivity of conducting polymers, since those materials are usually deposited as thin films and their conductivity range is not sufficient for two-point probe measurements. On the other hand the major problem in such estimations is establishing an ohmic contact between probes and sample. At a metal-semiconductor interface a potential barrier is formed inducing uncertainty in the measurement. Additional errors may rise due to differences in mechanical properties of wire probes and polymer surface.

Monitoring the changes in conductance during polymerization and doping reactions were done in a three electrode system utilizing a WE which was fabricated as a two-band electrode with a micrometer range spacing. As in typical conductometric measurements, between band electrodes with applied constant current, the voltage difference is recorded and related to the conductance. The growing electroactive film almost immediately covers the gap between the two bands, thus all the changes in resistance with increasing L_f value can be attributed to material deposition. This relationship can be described by the following logarithmic function [115]:

$$G \approx \frac{\sigma L_b}{\pi} \ln\left(\frac{8L_f}{\pi L_{sb}}\right) \quad (7)$$

Where: L_b and L_{sb} are the length and half spacing of the double-band electrodes respectively. Equation 7 is valid when L_f is greater than L_{sb} but also smaller than half of the total width of the double band electrode. In such a case sufficient coverage of the electrode and uniform growth of electroactive film can be assumed. For such geometrical conditions the current density (J) related to polymerization can be considered constant. Therefore, when the measured conductance increases linearly with increasing logarithm of polymerization time, then the obtained slope of the graph ($\sigma L_b/\pi$) equals to the conductivity of the synthesized film.

In situ conductance measurements as presented above can successfully be used in determination of electrical properties of conducting polymers and other electroactive materials. Electrical conductivity can be calculated from conductance vs. logarithm of

polymerization time plots, for films deposited during both potentiostatic and potentiodynamic electrosynthesis, with minimal information about films geometry needed. Additionally, this technique provides insight into changes in the conductance during doping reactions.

5.5. Potentiometric measurements

New materials synthesized or modified to fulfill certain requirements studied in this work were tested either as a template or solid contact material for ISEs. Fabricated sensors were used in potentiometric determination of lead which is a significant environmental pollutant. Typical potentiometric measurements are performed in a two electrode system as schematically shown in Figure 9 B. When two electrodes are immersed in an electrolyte, after a certain time equilibrium is reached and the potential of the cell (E_{cell}) is driven by a spontaneous redox reaction. If such a circuit is open (practically realized by high input impedance), then the current flow between WE and RE is minimal and therefore E_{cell} can be approximated to the difference of the work (W) conducted in the system divided by the difference in charge (q). Such an electrochemical system under these conditions is in fact a galvanic cell. Hence, the relationship between *emf* and activities of oxidized and reduced ions can be described by the Nernst equation. In potentiometry, both the formal and redox potential of RE are considered constant. Therefore, all the changes in *emf* can be related to the indicator electrode (*i.e.* WE) and the half-cell reaction at the electrolyte/ISM interface (Figure 15 A).

In the case where ISE consist of a conducting substrate and an ISM selective for specific cation, the Nernst equation can be expressed as:

$$emf \cong E^{0'} + \frac{\hat{R}T}{n_e F} \ln \frac{a_{x1}}{a_{x2}} \quad (8)$$

Where: \hat{R} is ideal gas constant equal to $8.3144621 \text{ J mol}^{-1} \text{ K}^{-1}$, F is the Faraday constant equal to 96485 C mol^{-1} , T is temperature in K. Activities of detected ion in solution and in ISM are symbolized by a_{x1} and a_{x2} , respectively (in units of concentration). The practical determination

of ion concentration in a solution is realized assuming that a_{x2} is constant. Hence, as can be seen from equation 8 the measured potential depends linearly with logarithm of the ion activity in solution enabling estimation of the concentration of ions of interest within dynamic range of the working sensor. Therefore, ISE can be considered as a logarithmic sensor.

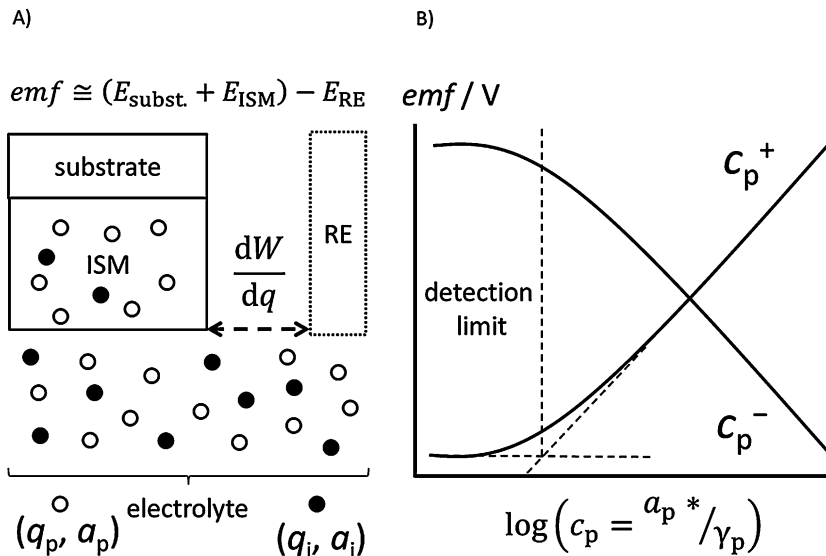


Figure 15. Schematic representation of the origin of emf in a two electrode system immersed in solution containing both primary and interfering ions (A). Calibration curves specific for cations and anions (B).

Idealized calibration curves specific for cations and anions are shown in Figure 15 B. The value of concentration obtained from potentiometric measurements for the primary ion (C_p) is dependent on two parameters: activity coefficient (γ_p) of the primary ion and selectivity constant of the membrane. The first one rely on ionic strength (overall ion-ion electrostatic interactions), thus this factor need to be constant in order to provide the linear logarithmic dependence of C_p on measured potential. The selectivity coefficient describes the influence of interfering ions which are present in the examined solution. Figure 15 A presents the case of two types of ions contributing to the analytical response of the ISE. Both the activity and charge of interfering ion influence the interaction of those ions with the ISM. The relationship

between emf , selectivity coefficient and the activity of primary and interfering ions is given by the Nikolskij-Eisenman semi-empirical equation [116]:

$$emf \cong const \pm 2.303 \frac{RT}{q_p F} \log \left(a_p + K_{p,i} a_i^{q_p/q_i} + LDL \right) \quad (9)$$

Where: LDL is the low detection limit, q_p and q_i are the charge number of primary and interfering ions, a_p and a_i are corresponding activities, and $K_{p,i}$ symbolize selectivity coefficient for this particular system. As can be seen from the above equation both $K_{p,i}$ and a_i can influence the detection limit of the working sensor. However, even if the activity of interfering ions is close to zero, the plateau region, schematically shown in Figure 15 B, will be still finally approached (with dilution) due to the reverse flux of primary ions from ISM to the solution. The major potentiometric characteristics of ISE taken into account during evaluation of the materials studied here are: LDL , slope of the line obtained during calibration procedure and hysteresis of the analytical response.

5.6. Surface characterization and deposition at nanoscale

The surfaces of deposited films were characterized by imaging techniques including scanning electron microscopy (SEM) and atomic force microscopy (AFM). Those techniques provide imaging with nanometer-resolution. In electron microscopy an image is produced by analyzing the interactions of a high energy electron beam with the examined surface. Depending on the actual need, the analytical signal in SEM can be divided to the so-called secondary and backscattered electrons which both can be used for imaging. The images obtained from backscattered electrons are used for SEM micrographs emphasized on the contrast in composition of the sample. Additionally, some of the fraction of backscattered electrons are diffracted according to Bragg's law (describing scattering from crystal lattice), yielding X-radiation (0.01 to 10 nm wavelength). Hence, a SEM instrument equipped with an energy-dispersive X-ray (EDX) analyzer can also give elemental analysis of the examined SEM image. The secondary electrons are in principle the generated electrons upon irradiation with energies higher than the ionization potential specific

for each element. The images obtained from ionized electrons yield the morphology of the microstructure, thus this analytical mode is the most frequently used in SEM imaging.

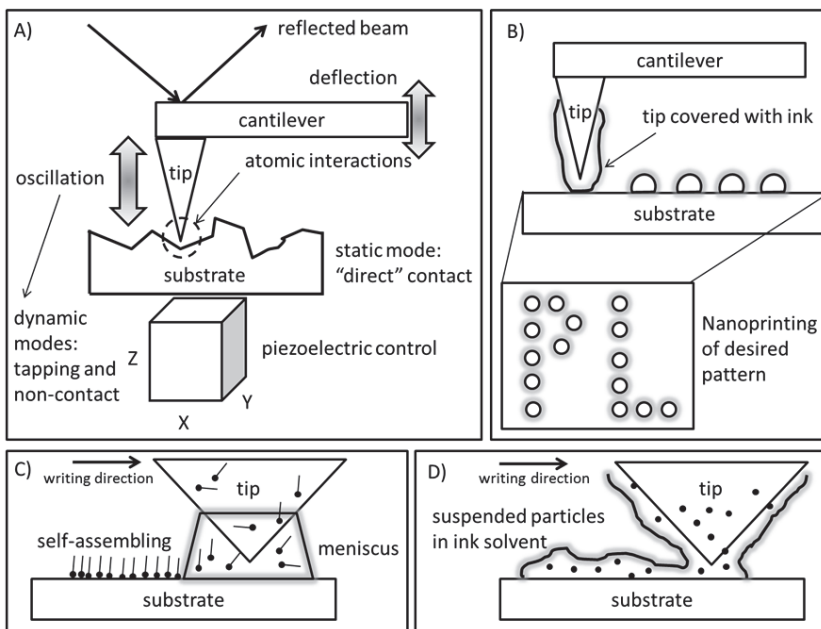


Figure 16. The principles of AFM imaging showing dynamic and static modes of operation (A). Schematic representation of nanoprining during DPN process (B) together with two distinct deposition mechanisms: a molecular transport facilitated by liquid meniscus formed between AFM tip and substrate (C), and solvent transfer from the tip to substrate using the ink carrier (D).

Both imaging and manipulation of matter at nanoscale can be done by scanning probe microscopy. The AFM technique in principle utilizes scanning probe which consist of a cantilever with a sharpest possible tip for imaging (Figure 16 A). The image is created by scanning a surface and monitoring the deflection of the cantilever which is induced by atomic interactions between the tip and the examined substrate. The deflection is typically related to the changes of the angle of a light beam illuminated over the end of the cantilever. The movement of the probe and/or mounted substrate in all directions is controlled by piezoelectric positioners. The feedback signal can be obtained by scanning with either a static or resonant cantilever which corresponds to the so-called contact and dynamic modes respectively. In the latter case, the cantilever-tip ensemble is excited at a fixed frequency and the measured amplitude is used as a feedback parameter. If a relatively stiff cantilever is

oscillated close to the sample the tip only intermittently touches the examined surface (the so-called tapping mode). In contrary, if the same tip is oscillated further away from the surface (*i.e.* non-contact mode) the majority of the measured forces between the tip and the surface are the van der Waals type. In the static contact mode cantilevers with a relatively low stiffness are used and the measuring probe is kept at constant height above the examined surface. There are several other operational modes currently available for AFM imaging based on the presented above basic modes, which are adjusted to fulfill certain measurement environments (*e.g.* imaging the samples exposed to liquids). With the state-of-the-art AFM instruments it is possible for some samples even to achieve atomic resolution.

The scanning probe technology can also be used in deposition of various materials at nanoscale in a form of lines or dots that could be arranged in desired patterns. This can be done by simply “dipping” the AFM tip into inks containing molecules that are to be deposited (Figure 16 B). The commercially available technique based on this principle is the so-called Dip-Pen Nanolithography (DPN). Transfer of ink/molecules from the tip to the substrate is limited mainly by contact time (*i.e.* dwell) and diffusion rate influenced by physiochemical properties of the depositing environment. There are two proposed mechanisms of deposition by DPN: the molecular transfer and physio-adsorption process (*vide* Figures 16 C and D, respectively). In the first one the molecules are delivered to the surface through a liquid meniscus. *E.g.* DPN-controlled deposition of thiols is driven by molecular diffusion yielding self-assembled monolayers on gold substrates [117]. It was found that the formation of water meniscus depends on the surrounding humidity [118]. On the other hand, for dispersions of nanoparticles, the deposition process is dependent on the nature and energy of the surface, therefore physio-adsorption related interactions are dominant [119]. DPN has been already used for the printing of *e.g.* proteins, metal nanoparticle and organic compounds [120] as well as exclusively conducting polymers [121-123]. Some of the AFM probes produced for DPN instruments are composed of multi-cantilever-tip ensembles. Hence, it is possible to simultaneously deposit different materials (*i.e.* multiplexing) at nanoscale with relatively high accuracy and precision. Additionally, patterning of multiplexed arrays can be extended over relatively large areas which is desirable *e.g.* in the fabrication of immunosensors [76].

6. Results and discussion

6.1. Electrochemistry of poly(*para*-phenylene) in room temperature ionic liquids

Electrochemical synthesis of conducting polymers assisted with RTILs typically results in enhanced electroactivity of the deposited films in comparison with classical organic solvents. Additionally, the material yield electrodeposited in RTILs in some cases, can be significantly higher. In **Paper I**, two RTILs representative for pyrrolidinium (R^1 =methyl, R^2 =butyl, “bmp”) and imidazolium (R^1 =methyl, R^2 =butyl, “bmim”) cations (*vide* Figure 11 A) combined with Tf_2N^- and PF_6^- anions respectively, were chosen as model RTILs for polymerization, doping and spectroelectrochemical studies of PPP. This conducting polymer is interesting for fundamental studies, since it can be both p- and n-doped to relatively high values. Also, chemical polymerization conditions of conducting polymers based on benzene can be optimized to obtain hyperbranched polymers (*i.e.* dendritic-like structures) [124]. Since electrochemical polymerization systems are non-deterministic with a considerable number of random variables, the resulting conducting polymers are in rather slightly branched than strictly linear forms. Application of new electrolytes may be useful in obtaining partial control over the electrochemical polymerization process to yield either relatively long conjugation length or branched (*i.e.* cross-linked) conducting polymers.

Selected RTILs (bmp Tf_2N and bmim PF_6) were compared with a conventional electrolyte containing 0.1 M TBAPF₆ in acetonitrile (ACN). Electrochemical polymerization of biphenyl was performed using CV within 0 and 1.8-1.9 V at 20 mV s⁻¹ scan rate during 10 consecutive cycles. As can be seen in Figure 17, potential scanning in bmim PF_6 resulted in far more complex shape of CV curves and a higher amount of material deposited compared to bmp Tf_2N and ACN (0.1 M TBAPF₆). Additionally, it can be suggested that the PPP film made in bmim PF_6 has a more rigid structure, since its redox response does not change significantly in biphenyl-free electrolyte during p-doping (*vide* CV curve number 4 in **Figure 3a** in **Paper I**).

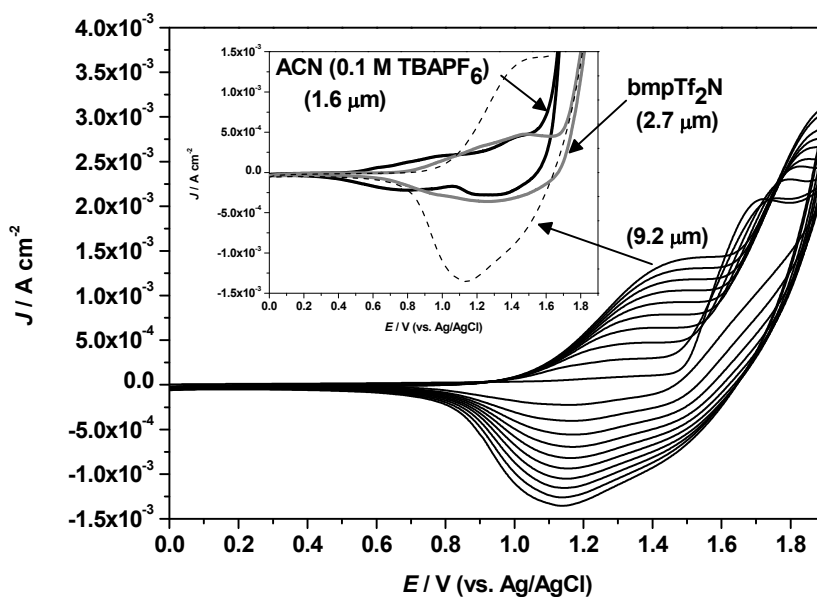


Figure 17. Cyclic voltammograms recorded during electrochemical polymerization of PPP in bmimPF₆ together with J/V curves obtained in bmpTf₂N and ACN (0.1 M TBAPF₆) presenting last scans of polymerization (shown in the insert). Note: the calculated apparent values of L_f (*vide* equation 10) are shown in the brackets.

The deposition efficiency can be estimated and discussed using the film growth rate. Therefore this parameter was chosen to compare the material yield obtained in the studied RTILs and in ACN (0.1 M TBAPF₆). The value of L_f can be determined according to the following equation [125]:

$$L_f = \frac{(Q_p M_m)}{(n_e F d_f A)} \quad (10)$$

Where: Q_p is the polymerization charge in C, M_m is the molecular weight of the monomer in g mol⁻¹ and d_f is the density of the film in g cm⁻³. Figure 17 shows the results of calculated L_f values (according to equation 10 and assuming that $d_f = 1$ g cm⁻³ and $n_e = 1$) for each electropolymerized film. In bmimPF₆ the value of the film growth rate is approx. 3- and 6-fold higher than in bmpTf₂N and ACN (0.1 M TBAPF₆), respectively.

The enhanced deposition rate for this particular ionic liquid over the other examined electrolytes can be induced by several factors like: viscosity, the stability of intermediate radicals, monomer concentration, differences in the applied potential (due to electrochemical windows specific for each electrolyte), solubility of oligomer products as well as the nature of counterions. Concentration of biphenyl was the same (50 mM) in bmimPF₆ and ACN (0.1 M TBAPF₆), thus this factor can be excluded from further considerations. Moreover, the Tf₂N⁻ anion has a negative effect on the polymerization process of PPP, since the optimal concentration of biphenyl for this RTIL was found to be around 100 mM.

In general, the preferable environment for synthesis of many organic compounds is rather acidic conditions defined as the presence of a Lewis acid (*i.e.* electron pair acceptor) [126]. ACN and Tf₂N⁻ can be considered as Lewis bases (*i.e.* electron pair donor) in contrast to PF₆⁻ or TBA⁺ ions. Additionally, the differences in the value of $E^{o'}$ for PPP in the examined electrolytes are only around 0.1 V and the stability of the intermediate radicals (schematically shown in Figure 8) is unknown. Therefore, a reasonable explanation for the greatly enhanced amount of deposited material in bmimPF₆ relies on the significant differences in viscosity (~4-fold over bmpTf₂N and presumably more than 800-fold over ACN). Relatively high viscosities of RTILs “translate” into lower than expected ionic conductivities (also influenced by not fully dissociated anions and cations [127]) as well as in slower diffusion and mass transport in comparison to conventional organic electrolytes. On the other hand, for any electrochemical process the most important is the WE/electrolyte interface. As already discussed in chapter 4.2, the higher concentration of reaction products in the vicinity of the electrode can directly be related to slower diffusion through RTILs.

The doping process of PPP made in bmimPF₆, bmpTf₂N and ACN (0.1 M TBAPF₆) was examined during potential dynamic studies in these electrolytes. Additionally, the *in situ* ATR-FTIR spectroscopy enabled more detailed analysis of energy spectra of PPP in comparison to recorded current/voltage and FTIR spectra alone. It was found that the p-doping response was enhanced in bmimPF₆ and n-doping in bmpTf₂N, compared to ACN (0.1 M TBAPF₆), as can be seen in *Figures 3 and 4* in **Paper I**. Those results are indicative for relatively higher redox

activity of deposited films in RTILs, especially because the CV curves for PPP made and doped in ACN (0.1 M TBAPF₆) suggest a slightly more capacitive response.

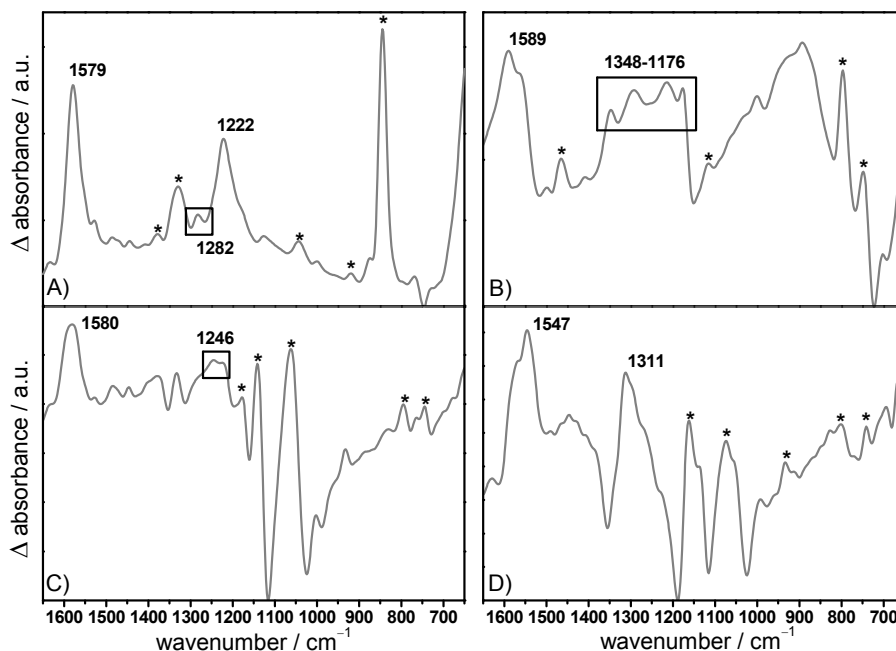


Figure 18. Selected *in situ* ATR-FTIR spectra of the PPP films made in the electrolytes studied in **Paper I** and correlated with the highest applied potential for each particular system. The difference spectra are within 1650-650 cm^{-1} wavenumber region and correspond to p-doping in ACN (0.1 M TBAPF₆) (A), in bmimPF₆ (B) and in bmpTf₂N (C), together with n-doping in bmpTf₂N (D).

Figure 18 shows the FTIR spectra corresponding to IRAV modes at high doping levels. In most of the studied cases, both the electronic absorption and the intensity of IRAVs raised significantly during redox reactions of PPP (*vide Figures 6 to 10 in Paper I*). The typical intense vibrations observed in the “fingerprint region” for benzene-based materials are roughly around 1600-1000 cm^{-1} which corresponds to C–C and C–H motions. For PPP, the Raman active vibrations in the doped state are at 1595, 1280 and 1220 cm^{-1} , together with IRAV modes at 1530, 1260 and 1180 cm^{-1} [128]. Since both the Raman and IR spectra of PPP can be discussed in the terms of effective conjugation coordinate theory (ECC), the frequency dispersion of some of the observed modes or their intensity relationships can be related to the conjugation length of polymer materials [128].

For PPP films made in ACN (0.1 M TBAPF₆) p-doping yielded the major IRAV modes at ~1579 and 1222 cm⁻¹ with significantly less intense peak at ~1282 cm⁻¹ (Figure 18 A). The relation in the intensity of the latter vibration to the peak at ~1222 cm⁻¹ suggests an extended conjugation length [129]. Although, much more material was deposited during polymerization of PPP in bmimPF₆, the resulting films are probably in a form of slightly branched and rigid polymer chains. For the films made and p-doped in bmimPF₆ the difference ATR-FTIR spectrum (Figure 18 B) exhibit multiple and relatively intensive peaks in the range 1348-1176 cm⁻¹ and a broad peak at ~1589 cm⁻¹ indicating a slightly rigid structure and a wide distribution of the conjugation lengths respectively [130,131]. As can be seen in Figure 18 C and in *Figure 3* in **Paper I**, the p-doping response in bmpTf₂N is not better than the films made and p-doped in ACN (0.1 M TBAPF₆), although slightly more material was deposited in this RTIL.

On the other hand, n-doping of PPP was only effective for films made and doped in bmpTf₂N. It was possible to reduce PPP in bmimPF₆. However, the changes upon doping of both the absorption and IRAV bands were insignificant (*vide Figures 9 A and B* in **Paper I**). The ATR-FTIR spectrum corresponding to approx. -2 V of applied potential is shown in Figure 18 D. This spectrum corresponds to the anionic form of PPP and exhibits two major vibrations at ~1547 and 1311 cm⁻¹. In contrary, the p-doped films correspond to cationic form of polymer. Hence, the spectral pattern, number of peaks and their position can be slightly different. Additionally, the doping process depends on the diffusion of ions through the electroactive films. Likewise, the size and nature of counterions can have either effective or defective impact on both the polymer structure and microstructure in terms of electrical properties and material stability. Therefore, a possible explanation of the enhanced electroactivity of PPP made and n-doped in bmpTf₂N can be related to the more balanced ratio between the molecular weight of cation and anion in this particular RTIL in contrary to electrolytes containing PF₆⁻ anion (*e.g. vide* common ions in RTILs presented in Figure 11).

The results presented in **Paper I** and selectively discussed in this chapter can be used in fundamental studies of conjugated materials in different directions. Both the electrochemical synthesis and electroactivity of conducting polymers can be greatly enhanced in RTILs in

comparison to conventional electrolytes, which was reflected in the polymerization and doping studies in the two representative ionic liquids: bmimPF₆ and bmitf₂N. Additionally, it was shown that spectroscopic studies of PPP in RTILs can be useful in revealing new features related to different structures of conducting polymers. This can be practically useful in discussion of the theoretical aspect of spectroscopic features of carbon-based aromatic electroactive materials.

6.2. Investigation of the water-soluble conducting polymer BBL derivatives

Charge transport efficiency in semiconducting materials is a key factor in the performance of electronic devices such as diodes and transistors. In polymer-based electronic devices, p-type semiconductors are mainly used, due to the lack of environmentally stable n-type conducting polymers [132]. Additionally, use of n-type semiconducting polymers in bipolar junctions or to fabricate ambipolar transistors, results in devices with relatively low field-effect mobility of electrons [133] in contrary to *e.g.* OFETs based on p-type PTs exhibiting relatively high mobility of holes [47]. One of the conducting polymers that can provide field-effect mobility of electrons at decent levels is the poly(benzimidazobenzophenanthroline) (BBL). Importantly, this ladder-type conducting polymer can be reversibly reduced chemically or electrochemically, yielding relatively high electrical conductivities [134]. For practical realization of all-plastic electronic devices there is a need for solution processable materials. However, BBL is insoluble in common organic solvents. From biosensor technology point of view it is beneficial to synthesize water soluble conducting polymers. Hence, in **Paper II**, BBL was functionalized with poly(ethyleneoxide) PEO side chains to obtain water-based inks.

Figure 19 presents the four BBL derivatives synthesized for this work, shown here as a function of the doping charge, together with a hypothetical BBL:PEO structure. The conjugation length has usually a positive impact on the electroactivity of conducting polymers and the length of side chains presumably increase the size of insulating regions within the polymer film. Therefore, the synthesized BBL derivatives had different BBL to PEO ratios, ranging from 1.8 up to 12 (*vide Table 1* in **Paper II**).

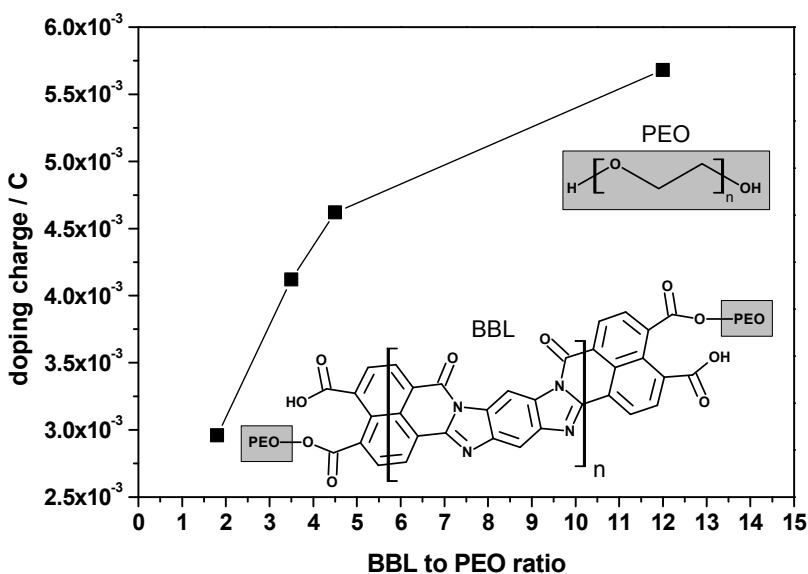


Figure 19. Studied PEO-functionalized conducting polymers based on BBL listed in *Table 1* in **Paper II**. The plot represents the BBL to PEO ratio in relation to the charge which past during n-doping of the polymers in ACN (0.1 M TBAPF₆) under potential cycling (*vide Figure 1* in **Paper II**). Note: the hypothetical structure of BBL functionalized with PEO side chains are shown as insert, and the straight lines between the points are shown only as a guide for the eye.

The n-doping response of drop casted BBL:PEO films was studied by CV in ACN (0.1 M TBAPF₆) under nitrogen atmosphere in order to study the influence of derivatization on both the relative film quality and electroactivity. The annealing effect on BBL:PEO films was investigated as well. According to *Tables 3 and 4* in **Paper II**, the overall doping charge that passed during n-doping of BBL:PEO films is independent of annealing. On the other hand, there is a clear relationship between the calculated doping charge and the BBL:PEO ratio. As can be seen in Figure 19, the BBL:PEO films exhibit enhanced electroactivity at higher BBL:PEO ratios. Hence, in order to achieve the optimal polymer structure and ink stability a proper balance between the side chains and the conjugation length needs to be considered. In this particular work BBL:PEO material with the highest number of BBL units and the shortest PEO side chains from the studied polymers was found to exhibit the highest electroactivity. However, since the

properties of BBL:PEO inks have not been studied it is unknown whether this particular BBL:PEO ratio is the optimal one in practical applications.

As can be seen in *Figure 1* in **Paper II** the BBL derivatives exhibit four clearly resolved redox processes. The n-doping response was studied additionally by *in situ* UV-vis spectroscopy (*Figures 5 and 7* in **Paper II**). Both the obtained current/voltage curves and the spectral patterns are very similar to the conventional BBL [134], indicating a minimal impact of side chains on the overall n-doping response. The calculated peak-to-peak potential separation ($E_p = E_{ox} - E_{red}$) was found to be independent on the BBL:PEO ratio. The value of E_p was, however, slightly smaller when BBL:PEO films were annealed (even at relatively low temperatures). Hence, presumably the size of separation regions created by extension of the side chains needed to be minimized. Also, it was found that annealing had an improving effect on the morphology of BBL:PEO films as can be seen in the AFM images presented in *Figure 4* in **Paper II**.

Importantly, BBL:PEO water based inks provided a significant improvement on processability of the BBL polymers in comparison to conventional BBL which is usually deposited from acidic solutions. Thus the results presented in **Paper II** are useful in understanding of the influence of functionalization of BBL in terms of future development of practical inks based on this particular ladder-type conducting polymer. On the other hand, the development of functional inks based on BBL derivatives needs a thorough study on their physiochemical properties as well as improvements in the air stability of the deposited films, in order to make a practical use of the concept presented and summarized in this chapter.

6.3. Synthesis, structure and electrochemistry of novel conducting films based on polycyclic aromatic hydrocarbons

Application of carbon-based materials that are structurally different from conducting polymers, with manifold functionality and properties adjusted to specific tasks is an attractive trend in sensor technology. The nanostructured materials ranging from different forms of carbon nanotubes and fullerenes to graphene, might be beneficial in the future sensor devices. Nevertheless, the complete integration of the electroactive transduction elements based on those materials, still represents a challenge, particularly in terms of cost-to-performance ratio, the overall sensor performance and functionality. To date there have been a tremendous number of scientific reports published on nanostructured carbon based materials connected also to specific sensor applications. However, very little is known on similar approaches using PAHs. Those molecules constitute probably the most widely spread organic group of compounds in the universe. Hence, proper focus on their possible future applications is definitely needed. The work presented in **Papers III and IV** is devoted mainly to the application of benzo(a)pyrene (BaP) as a monomer to obtain relatively larger PAH molecules and determination of the basic electrical properties of the resulted electroactive films. Since it is likely that the electrodeposited materials are a mixture of several PAH molecules with different sizes and symmetries, the name poly(benzopyrene) (PBP) has been adopted.

The structure of BaP is shown in Figure 10 A. Since BaP is one of the most studied PAH molecules, it was chosen as the model compound in fundamental studies on electrosynthesis and doping reactions of electroactive films based on PAHs. The first challenge connected with this research was in finding the optimal conditions for electrochemical synthesis of PBP by CV: a suitable organic solvent, monomer concentration and scan rate (*vide paragraph 3.1* in **Paper III**). It was found that the potential cycling from 0 to 1.4 V with 10 mV s^{-1} and in 20 mM concentration of BaP dissolved in PC (0.1 M TBAPF₆) yields a porous, reproducibly prepared and electrochemically stable electroactive films. Figure 20 shows a typical *J/V* curves obtained during electrosynthesis of PBP together with the recorded changes in the conductance of growing film. The electrical conductivity of the PBP films estimated by using the first part of

equation 7 (equivalent of *equation 1* in **Paper IV**) which is approx. equal to the slope of the G vs. $\ln(t)$ plot, is $\sim 6.6 \text{ mS cm}^{-1}$. This conductivity value places PBP films in the mid-semiconducting range.

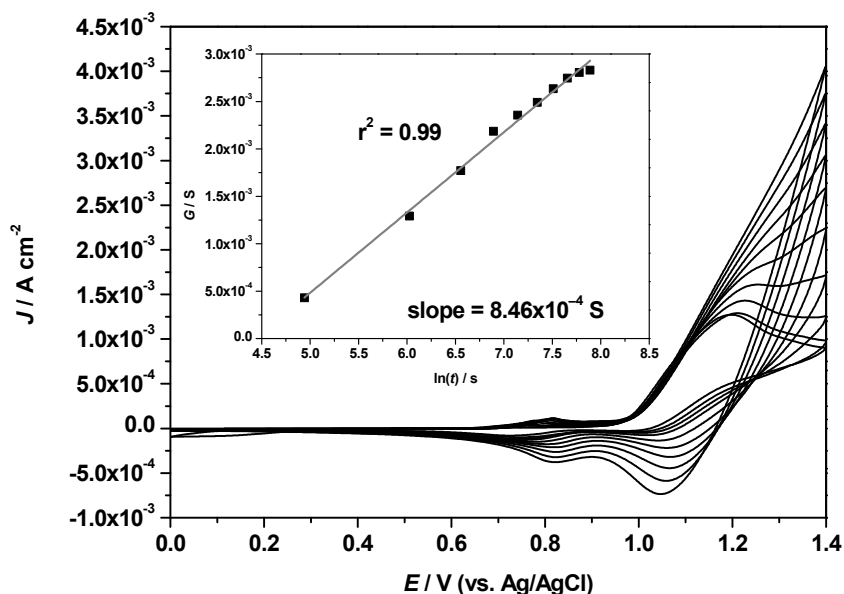


Figure 20. Electrochemical synthesis of PBP in PC (0.1 M TBAPF₆) together with corresponding *in situ* conductance measurements shown in the insert.

The second challenge relies on the exact determination of the basic constituents of the PBP films electrodeposited from BaP. This problem was examined by performing spectroscopic investigations presented in **Papers III and IV**. Since the polymerization product does not dissolve in any of the known solvents, the detailed structural analysis is very limited. Additionally, the obtained films are amorphous which excludes the X-ray diffraction analysis and disturbs the signal in transmission microscopy. Interestingly, kinetics of the doping response of the PBP films is different from any known charging processes confined by redox reactions. The PBP films are both p- and n-dopable exhibiting only reduction and re-oxidation peaks separated by $\sim 2.6 \text{ eV}$ energy difference. However, the magnitude of the recorded peak current is independent of the scan rate (*vide Figures 4 and 5* in **Paper III**). According to

equation 3, the value of I_p is in linear relationship with the square root of the scan rate and to fulfill this requirement the value of charge which passed during one potential scan need to be constant over different scan rates. The calculated charge corresponding to p- and n-doping of PBP at different scan rates is shown at Figure 21. In both cases the doping charge decreases exponentially with increasing scan rate. Therefore, with increasing scan rate, the amount of work required to move electrons across the film also need to decrease, indicating the existence of a highly conducting and ordered network. On the other hand, the value of the PBP “film resistance” (R_f) (*vide* measured conductivity) is in contradiction with this suggestion as well as observed amorphous microstructure.

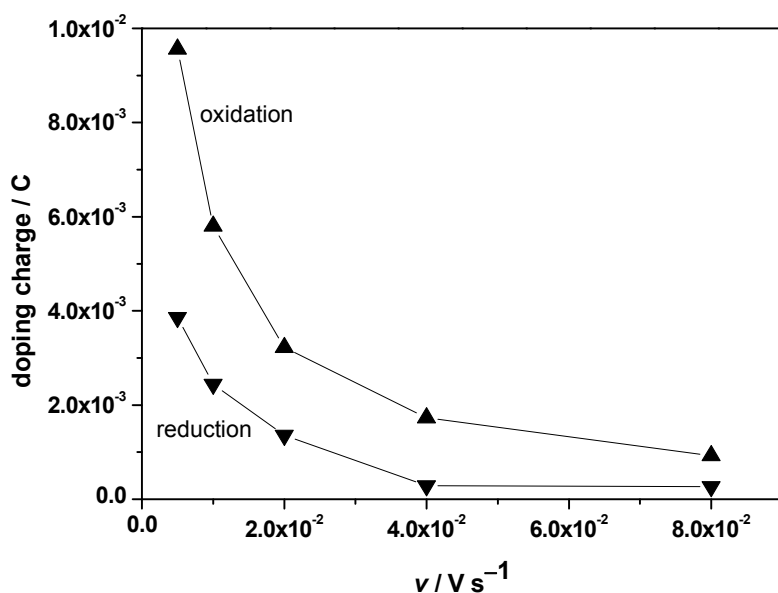


Figure 21. An example of the charge which passed during doping studies of PBP films (**Paper III**) shown as a function of scan rate. Note: the straight lines between presented points are shown only as a guide for the eye.

The unusual charging behavior of PBP films can be explained by a slow charging process at the electrolyte/film interface. Hence, this transmissive boundary needs to be dominated by heavily distributed centers of delocalized π -electrons originating from relatively large PAH molecules stacked together in the form of clusters. The absence of long-range order in PBP films most

probably originates from random arrangement of those molecular clusters as schematically shown in Figure 10 B. The assumptions about the structure of PBP are verified with the detailed analysis of both absorption and vibrational spectra of the PBP films. The estimated optical band gap is ~ 2.5 eV and the absorption maximum at ~ 420 nm (*vide Figure 6 in Paper III*). Since PAH molecules exhibit characteristic UV-vis spectra to high extent, those two values were confronted with the homologous series of PAHs.

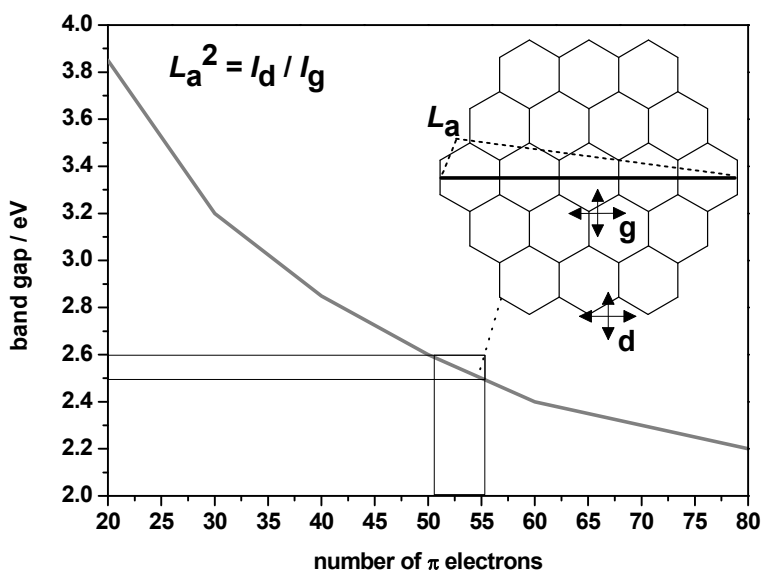


Figure 22. The number of π -electrons in a homologues series of PAH compounds as function of their optical band gaps according to [135]. The insert shows the crystallite length (L_a) in the relation of intensities of vibrations in the center of circumcoronene (I_g) and at the edges (I_d) interpreted as defects in “molecular graphene” [136].

As can be seen in Figure 22, the hypothetical average molecule in the PBP film consists of more than 50 π -electrons. The vibrational spectrum recorded *in situ* at the high oxidation state of PBP indicates that the average form of the molecule is similar to the cationic form of circumcoronene ($C_{54}H_{18}^+$). The structure of this compound is presented in Figure 10 A. Owing to the formal similarity of the PAH compounds to the surface confined graphene, the non-resonance Raman spectrum of PBP (*Figure 4 in Paper IV*) can be compared with the spectral

patterns consisting of two collective excitations (so-called “g” and “d” bands) characteristic to both graphene and graphite. Since the intensity of the “d” band rises with the increasing number of defects in the structure of graphene, the ratio between the intensity of the “d” and “g” bands (I_d/I_g) can be used to estimate the length of the analyzed molecule (L_a). The rough estimation of L_a according to the equation shown as an insert to Figure 22 yields approx. 1 nm, strongly indicating that the hypothetical average molecule in PBP films consist of 40 to 60 carbon atoms.

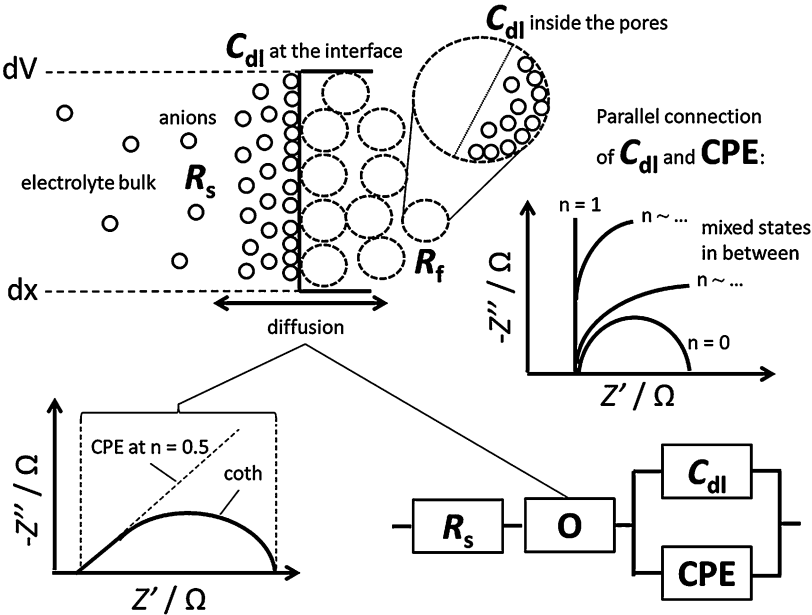


Figure 23. The proposed model of oxidation and charging of PBP films shown as a picture and equivalent circuit.

The equivalent circuit proposed in *paragraph 3.3* in **Paper IV** describes the electrochemical properties of PBP at different oxidation states with relatively high precision. Importantly, the average fitting error number (χ^2) for the developed model to recorded impedance spectra in two organic solvents (ACN and PC) with significantly different viscosities, is only $\sim 10^{-3}$ at high doping levels of PBP.

The mathematical description of this new equivalent circuit shown in Figure 23 is the following:

$$Y(\omega) = \frac{1}{R_s} + (Y_0\sqrt{j\omega}) \coth(B\sqrt{j\omega}) + Y_0(j\omega)^n(1 + j\omega C_{dl}) \quad (11)$$

Where: Y_0 is the magnitude of admittance in $S s^{1/2}$ and in $S s^n$ for O element and CPE respectively, B is the time constant related to diffusion in $s^{1/2}$ and n is the number describing the discrepancy of CPE from an ideal capacitor ($Y_0 = C$ if $n = 1$ and $Y_0 = R$ if $n = 0$). The parallel combination of C_{dl} , at both the interface and inside the pores with CPE, results in a powerful circuit which can cover the whole range of impedance spectra from a straight line to a semicircle. The addition of the O element to this circuit is beneficial in description of finite-length diffusion through transmissive boundary, especially at high doping levels of the PBP films. Verification of the model presented by equation 11 was made by direct comparison of the calculated and measured conductivity values estimated according to equation 7, at the four highest oxidation states of PBP films (*vide Figure 8* in **Paper IV**). The resultant slopes of the lines are almost identical for films doped in ACN (0.1 M TBAPF₆) strongly indicating that the model presented above sufficiently predicts the electrical properties of the PBP films. Therefore, it is an interesting alternative to the frequently used equivalent circuits based on the Randles model, due to its simplicity and flexibility in the description of “graphically different” impedance spectra.

The first attempt of the application of PAH-based electroactive materials in ISEs was presented in **Paper V**. BaP was mixed with the anion of the well-known complexometric indicator eriochrome black T (EbT) in ACN and relatively thin films were deposited on glassy carbon (GC) electrodes. EbT⁻ acted both as a dopant for the electrochemically generated PBP film and as a complexing agent toward lead ions, thus, yielding an ion-sensitive potentiometric sensor and a novel template material. The structure of the EbT⁻ anion is shown in the insert in Figure 24. Divalent cations interact with two oxygen functional groups and two nitrogens present in this planar molecule. The sulfonyl group in EbT⁻ provides electroneutrality in the PBP films and the planarity and notable delocalization of π -electrons around naphthalenic parts presumably

strongly affects the PBP cluster formation. Since the molecular weight of EbT^- is over 400 g mol^{-1} the mobility of this ion is significantly lower than *e.g.* PF_6^- , kinetics of the polymerization is affected and unusual polymerization pattern is obtained, as can be seen in *Figure 2* in **Paper V**. With each potential scan the total charge which passed in the system decreased, suggesting that the resistance value associated with mass transfer across the growing film is considerably high, probably owing to the affinity of naphthalenic parts of EbT^- to the wide spectrum of PAH molecules formed at the applied potential.

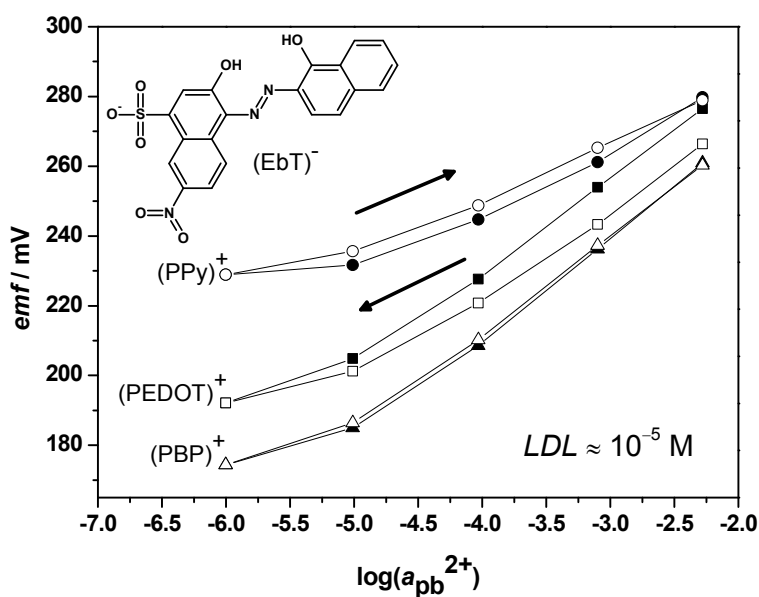


Figure 24. Potentiometric response of various GC/ Pb^{2+} -sensitive electrodes doped with EbT^- (shown as an insert) studied in **Paper V**. Note: the arrows refer to the direction of dilution/concentration (filled/unfilled symbols).

The PBP films made and doped with EbT^- were conditioned in lead (II) nitrate solution and their potentiometric response was compared with the corresponding *emf* recordings for both GC/PEDOT and GC/PPy films electrosynthesized in EbT water solutions. Calibration of the studied Pb^{2+} -sensitive sensors revealed that in the cases of both GC/PEDOT- EbT and GC/PBP- EbT electrodes, a typical detection limit was obtained. However, the GC/PBP- EbT sensor was ready to use already after one day of conditioning, in contrary to PEDOT-based electrodes

which require two days and a constant sub-Nernstian response of GC/PPy-EbT electrodes. Moreover, the hysteresis effect of the Pb^{2+} -sensitive films as shown in Figure 24 of the GC/PBP-EbT electrodes is rather small, thus placing these electrodes close to conventional solid-state $\text{PbS}/\text{Ag}_2\text{S}$ electrode in terms of *emf* measurement stability. The relatively stable and fast potentiometric response of the GC/PBP-EbT electrodes can be attributed to both the structure and microstructure of PBP-EbT films as well as a relatively small thickness of the films obtained in **Paper V**, in comparison to typical conducting polymers-based films or PBP made in PC (0.1 M TBAPF₆) that exhibited an extraordinarily high film growth rate.

The presence of lead in PBP doped with EbT after soaking in lead (II) nitrate solution was confirmed by EDX analysis of the studied films (*vide Figure 11* in **Paper V**). Therefore, presumably other eriochrome-type compounds can also be selected for making PAH-based templates selective for other divalent cations like Mg^{2+} or Ca^{2+} (detection of which is potentially important in bio-related applications). Also, since EbT^- is a dye which forms a red chelate with metal ions (in contrary to blue color of free dye), electrodeposited thin layer of this template material with immobilized EbT, might be useful in optical sensors. PBP-EbT films were already successfully used as an ion-to-electron transducer in ISEs in lowering of the detection limit of Pb^{2+} -ISEs [137].

One-step electrochemical synthesis of carbon-based, rigid in structure and porous conducting templates starting from relatively small PAHs was discussed in this chapter. The novel electrical model describes accurately the oxidation states of PBP, showing the existence of a semiconducting amorphous network with physicochemical properties facilitating relatively fast ion transport. Since presumably different kinds of primary and secondary dopants can be embodied into herein studied materials, the PAH-based films can achieve versatile functionality which could be potentially useful in future chemical sensors or in electrocatalytic applications.

6.4. Development of water-based PEDOT:PSS inks for nanoprinting and durable chemical sensors

Practical realization of conducting polymer-based devices depends to a large extent on the processability of those materials. Industrial or even laboratory scale production demands materials that can be embodied into manufacturing processes in a reproducible and reliable way. Since most practical deposition methods are lithography-related, there is a need for the development of new inks that would provide sufficient functionality and exhibit suitable physical properties for printing. Functional design of inks containing electroactive species mainly concentrates on the tuning of electrical conductivity of printed material despite the concern about ink properties (*e.g.* viscosity) for printing purposes. Especially for sensor applications the deposited conducting polymer films should have relatively low impedances. The other less explored, however, desirable functionality of conducting polymer-based inks, is connected with the long-term stability of electroactive deposits in certain fluids. The work presented in **Paper VI** is devoted to the issues connected with adhesion of PEDOT:PSS films on electrode substrates in aqueous environments, however, still utilizing water-based inks for casting. As already mentioned in paragraph 2.3, conducting PEDOT can be synthesized together with PSS surfactant yielding material with relatively high solution processability. From sensor technology point of view this particular conducting polymer is an attractive functional material mostly due to its relatively low redox potentials combined with sufficient electrochemical stability [36]. Moreover, PEDOT:PSS exhibit a tolerable level of biocompatibility [138].

Thin films of PEDOT:PSS can electrochemically be synthesized, thus providing a relatively easy way of making functional chemical sensors on existing electrode patterns. In such a case the adhesion of the PEDOT:PSS films to the various conducting substrates in aqueous media is usually sufficient. On the other hand, the adhesion of solution cast PEDOT:PSS to different surfaces in water is very limited [139], thus leading to severe restrictions *e.g.* in bio-related applications or ion detection in environmental samples. About half of the sulfonyl groups in the PSS polyanion are not involved in the doping of PEDOT [140]. Therefore, PEDOT:PSS in water is in the form of particles consisting of a PEDOT-rich core and PSS-rich outer shell.

Consequently, multivalent cations can be used as cross-linkers, yielding 3 D networks of hydrogel which can facilitate relatively fast ion transport [139]. The stability of gelled PEDOT:PSS in water is usually enhanced in comparison to the non-modified PEDOT:PSS films. Presumably, a similar effect exists for monovalent cation additions with hydrophobic chains. At sub-particle level the cross-linking cation exchanges with Na^+ and H^+ which are present in the sulfonic groups in the PSS polyanion. It was reported that the additions of quaternary ammonium cations can significantly reduce the solubility of PEDOT:PSS in water [141]. The reason for this is probably manifold, however, one can suggest cation exchange mechanism (*vide* insert in Figure 25) and interaction of PSS-rich outer shells with quaternary ammonium cation-based micelles.

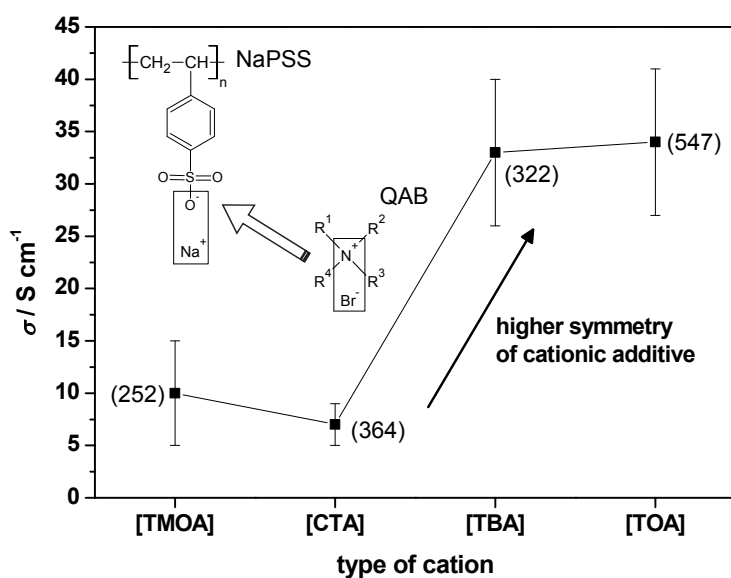


Figure 25. The graph representing the impact of QAB salts on the electrical conductivity of PEDOT:PSS films (according to *Table 2* in **Paper VI**). Notes: the insert shows the hypothetical interaction between polyanionic PSS and studied cationic ammonium additives together with their corresponding molecular weights in g mol^{-1} , shown in the brackets.

Since both the molecular weight and symmetry of quaternary ammonium cations can influence the arrangement of PSS chains, the following quaternary ammonium bromide (QAB) salts were

studied in **Paper VI**: trimetyloctylammonium (R^{1-3} =methyl, R^4 =octyl, “TMOA”), hexadecyltrimethylammonium (R^{1-3} =methyl, R^4 =hexadecyl, “CTA”), tetrabutylammonium (R^{1-4} =butyl “TBA”) and tetraoctylammonium (R^{1-4} =octyl “TOA”). Those salts were dissolved in ethylene glycol (EG) to yield 0.05 M solutions which were used as soaking media of PEDOT:PSS deposits on GC electrodes. Addition of polyalcohols is known to significantly increase the electrical conductivity of PEDOT:PSS *via* a secondary doping mechanism which leads to the decrease in thickness of the PSS barrier separating the PEDOT-rich grains [142]. Presumably, the number of polar groups in polyalcohol can have an effective impact on the overall conductivity, thus, QAB salts might exhibit a similar feature. Since the selected additives studied in **Paper VI**, were also intended to meet requirements regarding printing, the EG was chosen due to its sufficient thickening properties and the ability to effectively dissolve a wider range of QAB salts than other more viscous polyalcohols. Also, addition of surfactants in the form of QABs is highly beneficial. As can be seen in *Table 2* in **Paper VI** and Figure 25, all studied EG-QAB modifiers resulted in enhanced conductivity of the PEDOT:PSS films. However, the cations with higher symmetry were found to be more effective in optimization of PEDOT chains toward higher conductivities.

A highly important finding regarding the GC/PEDOT:PSS electrodes modified with EG-QABs is connected with their outstanding durability in aqueous solutions (also with low pH values). As can be seen from *Figures 1 and 2* in **Paper VI**, the studied systems survived 60 days of constant soaking in citrate buffer (pH 4) with minimal decrease in electroactivity. In order to quantify the transport dynamics of those electrochemical systems, several EIS measurements were performed. Recorded impedance spectra were fitted to the model composed of a resistor connected in series with a T element. The mathematical description of this model is presented below:

$$Y(\omega) = \frac{1}{R_s} + (Y_0\sqrt{j\omega})\tanh(B\sqrt{j\omega}) \quad (12)$$

Since PEDOT:PSS exhibits capacitor-like behavior, the impedance spectra (shown as Nyquist plot) of EG-QAB-modified PEDOT:PSS electrodes were dominated by a vertical line (reflective

boundary) with a minimal influence from diffusion. It is convenient to use the T element for the description of oxidation and capacitive charging of the PEDOT:PSS films, due to the fact that at low frequencies this element is equivalent to a resistor (R_d) and capacitor ($C_d = Y_0 B$) connected in series and at high frequencies it resembles the Warburg impedance as can be seen in the insert in Figure 26).

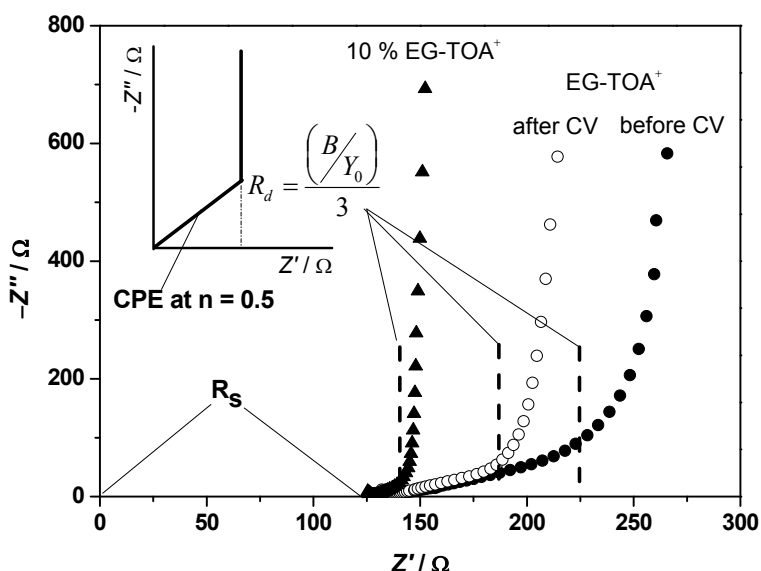


Figure 26. Nyquist plot representing typical recorded impedance of GC/PEDOT:PSS electrodes modified with EG-TOA⁺ (selected among studied additives in **Paper VI** and shown as an example). Note: a schematic explanation/interpretation of the model described by equation 12 is shown as insert.

According to the results presented in *paragraph 3.3* in **Paper VI**, all recorded impedance spectra for modified GC/PEDOT:PSS electrodes exhibited very similar characteristics, except the films soaked in EG-TOA⁺, for which the extended diffusion lines were observed. Interestingly, the calculated diffusional time constant for those films significantly decreased after CV was performed. This effect was not observed when EG-TOA⁺ (10 volume %) was mixed directly with the PEDOT:PSS ink before casting (Figure 26). A possible explanation for this phenomenon can be related to existence of a specific “blocking structures” at the PSS outer-

shells facilitated by both relatively long chains and branched TOA⁺ cations. Those specific structures might be influenced by ion transport into and out of the film during potential cycling. The PEDOT:PSS films casted from inks containing 10 volume % of EG-TOA⁺ were annealed before exposure to water and the conductivity of those films were slightly higher than films modified by soaking. Thus, the following suggestion can be made that the applied temperature (~100 °C) further decreased the distance between the individual PEDOT:PSS particles. The calculated apparent diffusion coefficient utilizing the constant B (*vide* equation 12) and estimated film thickness of ~10 μm, is in the range of 10⁻⁶-10⁻⁵ cm² s⁻¹, indicating that PEDOT:PSS films modified with EG-QAB are likely to be in the form of swollen hydrogels which facilitates ion transfer.

The more practical approach for modification of PEDOT:PSS films other than soaking is the direct addition of the modifier to the ink. However, it was found that only the addition of TOA⁺ cation provided enhanced adhesion. Therefore, this QAB salt could be considered in designing a variety of water-based PEDOT:PSS inks that could be utilized for *e.g.* ink-jet printing. Nevertheless, all of the studied modified PEDOT:PSS films were tested as a solid-contact material in Pb²⁺-ISEs (*Figure 5* in **Paper VI**). Only the films modified with EG-CTA⁺ and EG-TOA⁺ exhibited instant close-to-Nernstian response with LDL of ~10⁻⁷ M, after 2 days of conditioning in lead (II) nitrate. *Figure 27* presents a comparison between the potentiometric response of the GC/PEDOT:PSS/PVC-based Pb²⁺-ISE electrodes where the solid-contact was modified by soaking in EG-TOA⁺ and of conventional solid-state PbS/Ag₂S electrode. The modification of PEDOT:PSS seems to be beneficial, since both LDL and measurement uncertainty at low activity of Pb²⁺ are improved. The insert in *Figure 27* shows the corresponding response of an electrode with the PEDOT:PSS solid-contact that was modified by 10 % volume addition of EG-TOA⁺ to the ink. Similar characteristic in terms of the slope and LDL were obtained after several measurements and it has to be concluded that the sensor based on 10 % volume addition of EG-TOA⁺ at this stage of the research cannot be used instantaneously after conditioning. On the other hand, after 10 days potential stability test of the solid-contact Pb²⁺-

ISEs in buffer solution (\sim pH 4) containing lead ions (*Figure 4* in **Paper VI**), only the electrode with 10 % EG-TOA⁺ provided the slope of 27 mV dec⁻¹ and *LDL* of 10⁻⁷ M.

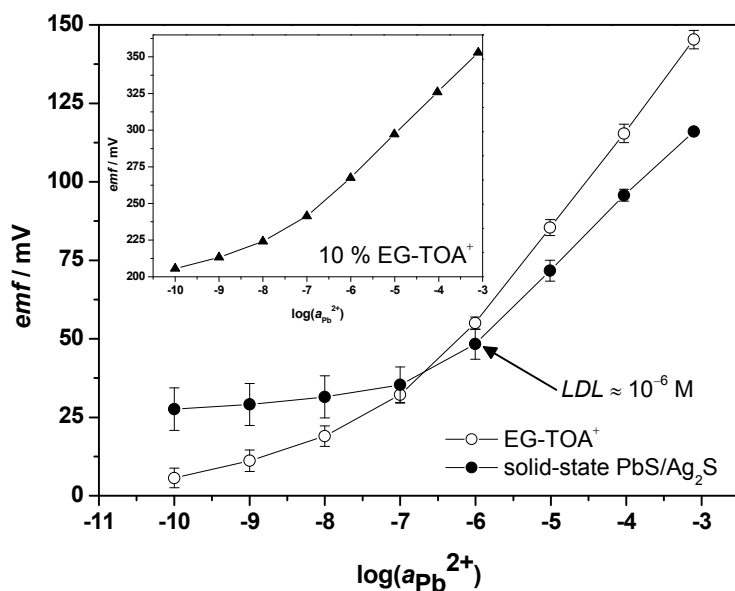


Figure 27. Calibration curves for GC/PEDOT:PSS/PCV-based Pb²⁺-ISE electrode where the interlayer of PEDOT:PSS was modified by soaking in EG-TOA⁺ and for conventional solid-state PbS/Ag₂S electrode. Notes: the insert presents the calibration curve for GC/PEDOT:PSS/PCV-based Pb²⁺-ISE electrode (where PEDOT:PSS interlayer was casted from PEDOT:PSS ink directly mixed with 10 % EG-TOA⁺) obtained after several calibrations (according to *Figure 5* in **Paper VI**).

Development of water-based PEDOT:PSS inks for nanoprinting where the major additive is a polyalcohol, is presented in **Paper VII**. In this work, the arrays of PEDOT:PSS dots were obtained utilizing DPN. The application of glycerol and two different surfactants enabled stable patterning of PEDOT:PSS where the single printed dot was scaled-down to nearly a nanodomain. An example of a printed array on silicon is shown as the insert in Figure 28. This AFM image shows a part of 81 printed dots within one 40x40 μ m array. The DPN probes used in this work have 12 tips, thus at the same time multiple arrays were printed and moreover it is possible to cover macro-scale areas with the desired patterns. The majority of the research regarding DPN is concentrated to print immunosensors and for this configuration the

deposition of desired moieties is driven by molecular transport facilitated by water meniscus formed between the tip and substrate. For the other inks containing extensive amount of nanoparticles, the mass transfer is governed by processes related to physio-adsorption. For those two proposed deposition mechanisms schematically shown in Figures 16 C and D, the different composition of inks needs to be considered. The deposition of *e.g.* relatively small molecules or nanoparticles does not need significant adjustment of ink properties, since the influence of dispersed moieties on the overall viscosity and ink stability during printing is minimal. Therefore, nanoprinting of dispersed conducting polymers is challenging, due to the considerable sizes of conducting particles and their complex interactions with the surrounding environment.

The selective patterning of PEDOT:PSS arrays *via* DPN to complement the ink-jet printing, may be useful in applications such as, for example, chemical sensors with enhanced signal-to-noise ratio or as hosts for living cells with the possibility to electrically stimulate them. Figures 28 A and B presents the obtained dot dimensions for the first attempts to deposit PEDOT:PSS with DPN. The commercial PEDOT:PSS water-based inks without any modification did not give reproducible DPN printing. Hence, in one approach the whole set of tips was dipped to the mixtures of PEDOT:PSS and methanol, yielding gelated structures [123]. In such a case, an average dot width is at 1-1.2 μm level, similarly when Mg^{2+} cations were used as additional cross-linker. Depending on conditions that are difficult to control it was possible to scale down the dot widths to 800 or even to 600 nm. However, since in DPN extremely small volumes of ink are used, any changes in surrounding environment highly influence both ink and printing stability. Additionally, these printed nanoarrays do not survive after exposure to water. Therefore, in order to provide a reproducible patterning from PEDOT:PSS, a more rational ink design was needed.

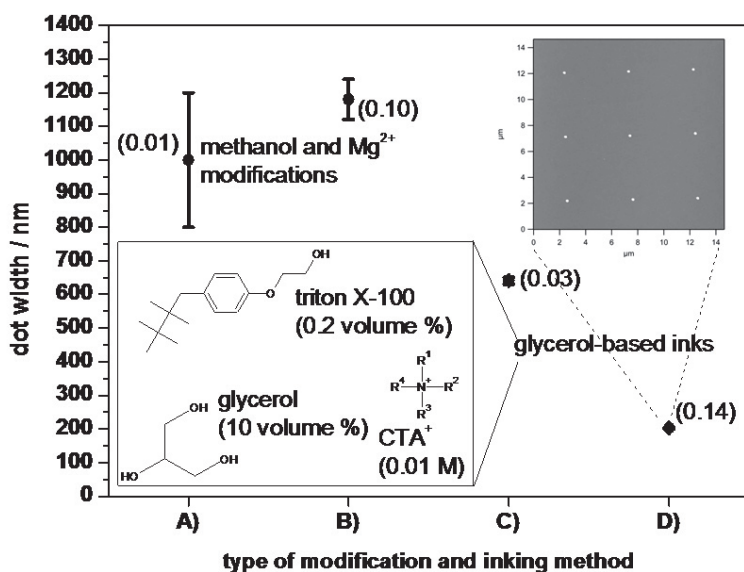


Figure 28. Comparison of the dot widths in patterned PEDOT:PSS *via* DPN (dwell time = 1 s) on silicon surfaces selected as an example of different inking procedures and ink modifications. Dipping of the whole set of tips in PEDOT:PSS/methanol (1:2) water solution (A) together with pre-dipping of corresponding set of tips in 25 mM Mg_2SO_4 (B) results in dot widths around 1 μm and a notable standard deviation [123]. The glycerol-based inks developed in **Paper VII**, utilizing commercial (C) and in-house synthesized (D) PEDOT:PSS. Note: an example of printed nanoarray, together with the ink additives and their concentration in studied PEDOT:PSS inks are shown as inserts. Additionally, the estimated aspect ratio between the dot height and width is shown in the brackets.

In the insert in Figure 28, a successful ink composition is presented (according to **Paper VII**). Each ink component has its own function in synergistic approach. Triton X-100 is a well-known nonionic surfactant that is widely used in industry, herein enhancing the dispersion of PEDOT:PSS particles and significantly lowering the surface tension of the ink (*i.e.* improvement in wetting of the tip). Addition of glycerol provides ink stability during printing by having a defective influence on the rate of ink evaporation. Also, this polyalcohol enhance the conductivity of PEDOT:PSS deposits in a similar manner as EG modifiers already discussed in this chapter. CTA^+ cations was dissolved in glycerol providing after-deposition enhanced adhesion of PEDOT:PSS in water, as well as being an additional dispersant. For those glycerol-

based inks a significant improvement in the scaling-down of dot dimensions was observed (*vide* Figures 28 C and D). With certain dwell times it was possible to print dots with less than 200 nm in diameter as can be observed in *Figure 4* in **Paper VII**. Importantly, the standard deviation of the dot dimensions indicates the degree of uniformity and reproducibility of the patterning, which is also similar to that reported during DPN printing of thiols and acid monolayers deposited on gold [143] for which the deposition is facilitated by the formation of a water meniscus. This significant improvement was obtained on both silicon and gold substrates by utilizing in-house synthesized PEDOT:PSS instead of the commercial material. The calculated aspect ratios (shown in Figure 28) for in-house synthesized PEDOT:PSS-based inks is ~5-fold larger in comparison to commercial PEDOT:PSS-based inks discussed in this work. This indicates that by proper adjustment of the ratio of PEDOT to PSS to be used in chemical synthesis, notable more material can be delivered at nano-confined volumes.

This chapter aimed to summarize the research on modification of PEDOT:PSS films with relatively large cations and polyalcohols. The addition of QAB salts resulted in cross-linked PEDOT:PSS particles and in enhanced adhesion and conductivity of the PEDOT:PSS deposited. It was found that with the use of relatively easy protocols for obtaining PEDOT:PSS water-based inks it is possible to obtain durable chemical sensors with sufficient recognition characteristics as well as arrays of conducting polymers with nanoscale features.

7. Final summary and possible future directions

The fundamental studies conducted on π -conjugated systems, discussed in this work, affirmed the importance of electrochemistry as a set of “principles and tools” that are useful in implementation of new ideas in sensor science. Since one can predict that in the near future organic electronics will be tightly connected with sensor technology, the results presented above (especially on ink development and PAH-based structures) might form a solid basis for further development of new commercial functional devices.

OFETs in integrated circuits and scaled-down to nanometer range could be the future of chemical sensing, bioelectronics or in energy storage and conversion applications. This would be possible by tuning the properties of conducting polymer based-inks for *e.g.* ink-jet printing. It was shown in **Papers VI and VII** that by a proper selection of cationic surfactants and polyalcohols one can obtain the desired synergy of ink additives for a particular printing process and application. Also, the characterization studies were performed on n-type conducting BBL derivatives (**Paper II**) which are meant for water-based inks suitable to deposit active layers in *e.g.* OFETs. The development of different conducting polymer water-based inks is useful in getting closer to printing of biomolecules and implementing them into recognition processes in bio-related applications.

The electroactivity of functional layers in chemical sensors based on electrosynthesized conducting polymers can be elevated by utilization of ionic liquid electrolytes. Some of the issues connected with this concept, were explored in **Paper I**. Also, ionic liquids with relatively high viscosity might be employed for electrochemical synthesis of larger PAH structures, resulting in even better electroactive templates than presented and characterized in **Papers III and IV**. Importantly, the developed electrical model describing different oxidation states of PBP films can presumably be utilized for other porous electrified templates or networks, providing sufficient and reliable approximation of reality. In addition to the synthesis and characterization of electroactive materials, the concepts of utilization of new templates and modifiers in chemical sensing (particularly for ISEs) have been affirmed in **Papers V and VI**.

List of references

- 1 H. Shirakawa, E. J. Louis, A. G. MacDiarmid, C. K. Chiang and A. J. Heeger, "Synthesis of electrically conducting organic polymers: halogen derivatives of polyacetylene, $(\text{CH})_x$ ", *Journal of the Chemical Society, Chemical Communications*, 16 (1977) 578–580.
- 2 B. A. Bolto, R. McNeill and D. E. Weiss, "Electronic Conduction in Polymers. III. Electronic Properties of Polypyrrole", *Australian Journal of Chemistry*, 16 (1963) 1090–1103.
- 3 C. K. Chiang, S. C. Gau, C. R. Fincher, Y. W. Park, A. G. MacDiarmid and A. J. Heeger, "Polyacetylene, $(\text{CH})_x$: n-type and p-type doping and compensation", *Applied Physics Letters*, 33 (1978) 18–20.
- 4 A. J. Heeger, A. G. MacDiarmid and H. Shirakawa, "The Nobel Prize in Chemistry, 2000: Conductive polymers", advance information of the Royal Swedish Academy of Sciences
- 5 W. R. Salaneck, R. H. Friend and J. L. Bredas, "Electronic structure of conjugated polymers: consequences of electron-lattice coupling", *Physics Reports*, 319 (1999) 231–251.
- 6 A. J. Heeger, "Disorder-Induced Metal–Insulator Transition in Conducting Polymers", *Journal of Superconductivity*, 14 (2001) 261–268.
- 7 M. Rohwerder and A. Michalik, "Conducting polymers for corrosion protection: What makes the difference between failure and success?", *Electrochimica Acta*, 53 (2007) 1300–1313.
- 8 K. Gurunathan, A. Vadivel Murugan, R. Marimuthu, U. P. Mulik, D. P. Amalnerkar, "Electrochemically synthesised conducting polymeric materials for applications towards technology in electronics, optoelectronics and energy storage devices", *Materials Chemistry and Physics*, 61 (1999) 173–191.
- 9 J. Janata and M. Josowicz, "Conducting polymers in electronic chemical sensors", *Nature Materials*, 2 (2003) 19–24.
- 10 U. Lange, N. V. Roznyatovskaya and V. M. Mirsky, "Chemical polymers in chemical sensors and arrays", *Analytica Chimica Acta*, 614 (2008) 1–26.
- 11 L. Rothberg, T. M. Jedju, S. Etemad and G. L. Baker, "Dynamics of Photogenerated Solitons in Trans-Polyacetylene", *Journal of Quantum Electronics*, 24 (1988) 311–314.
- 12 J. L. Bredas and G. B. Street, "Polarons, Bipolarons, and Solitons in Conducting Polymers", *Accounts of Chemical Research*, 18 (1985) 309–315.
- 13 J.-F. Chang, H. Sirringhaus, M. Giles, M. Heeney and I. McCulloch, "Relative importance of polaron activation and disorder on charge transport in high-mobility conjugated polymer field-effect transistors", *Physical Review B*, 76 (2007) 205204.
- 14 V. I. Arkhipov, E. V. Emelianova and G. J. Adriaenssens, "Effective transport energy versus the energy of most probable jumps in disordered hopping systems", *Physical Review B*, 64 (2001) 125125.

- 15 M. Yamaura, T. Hagiwara and K. Iwata, "Enhancement of electrical conductivity of polypyrrole film by stretching: Counter ion effect", *Synthetic Metals*, 26 (1988) 209–224.
- 16 A. J. Epstein, J. Joo, R.S. Kohlman, G. Du, A.G. MacDiarmid, E. J. Oh, Y. Min, J. Tsukamoto, H. Kaneko and J. P. Pouget, " Inhomogeneous disorder and the modified Drude metallic state of conducting polymers", *Synthetic Metals*, 65 (1994) 149–157.
- 17 V. N. Prigodin and A. J. Epstein, "Quantum hopping in metallic polymers", *Physica B*, 338 (2003) 310–317.
- 18 J. L. Bredas, J. Cornil, and A. J. Heeger, "The Exciton Binding Energy in Luminescent Conjugated Polymers", *Advanced Materials*, 8 (1996) 447–452.
- 19 F. Cacialli, R. H. Friend, S.C. Moratti and A. B. Holmes, " Characterization of properties of polymeric light-emitting diodes over extended periods", *Synthetic Metals*, 67 (1994) 157–160.
- 20 L. Dai, "Advanced syntheses and microfabrications of conjugated polymers, C₆₀-containing polymers and carbon nanotubes for optoelectronic applications", *Polymers for Advanced Technologies*, 10 (1999) 357–420.
- 21 N. C. Greenham and R. H. Friend, "Semiconductor Device Physics of Conjugated Polymers", *Solid State Physics*, 49 (1996) 1–149.
- 22 P. L. Burn, A. Kraft, D. R. Baigent, D. D. C. Bradly, A. R. Brown, R. H. Friend and R. W. Gymer, "Chemical tuning of electroluminescent copolymers to improve emission efficiencies and allow patterning", *Nature* 356 (1992) 47–49.
- 23 N. C. Greenham, S. C. Moratti, D. D. C. Bradlay, R. H. Friend and A. B. Holmes, "Efficient light-emitting diodes based on polymers with high electron affinities", *Nature* 365 (1993) 628–630.
- 24 C. Kvarnström and A. Ivaska, "Spectroelectrochemical study of polyphenylene by *in situ* external reflection FT-IR spectroscopy I. Polymerization of biphenyl", *Synthetic Metals*, 62 (1994) 125–131.
- 25 D. Dini, F. Decker and G. Zotti, "Electrochemical Growth of Polyalkylthiophenes. In Situ Characterization of Deposition Processes", *Electrochemical and Solid-State Letters*, 1 (1998) 217–219.
- 26 J. Heinze, B. A. Frontana-Urbe and S. Ludwigs, "Electrochemistry of Conducting Polymers-Persistent Models and New Concepts", *Chemical Review*, 110 (2010) 4724–4771.
- 27 E. M. Genies, G. Bidan and A. F. Diaz, "Spectroelectrochemical study of polypyrrole films", *Journal of Electroanalytical Chemistry*, 149 (1983) 101–113.
- 28 H. Young and A. J. Bard, "The application of fast scan cyclic voltammetry. Mechanistic study of the initial stage of electropolymerization of aniline in aqueous solutions" *Journal of Electroanalytical Chemistry*, 339 (1992) 423–449.

- 29 G. A. Sotzing, J. R. Reynolds and P. J. Steel, "Poly(3,4-ethylenedioxythiophene) (PEDOT) prepared via electrochemical polymerization of EDOT, 2,2'-Bis(3,4-ethylenedioxythiophene) (BiEDOT), and their TMS derivatives", *Advanced Materials*, 9 (1997) 795–798.
- 30 F. L. Klavetter and R. H. Grubbs, "Polycyclooctatetraene (polyacetylene): synthesis and properties", *Journal of the American Chemical Society*, 110 (1988) 7807–7813.
- 31 S. A. Jenekhe and P. O. Johnson, "Complexation-mediated solubilization and processing of rigid-chain and ladder polymers in aprotic organic solvents", *Macromolecules*, 23 (1990) 4419–4429.
- 32 U. Scherf and K. Müllen, "Poly(arylenes) and poly(arylenevinylenes). 11. A modified two-step route to soluble phenylene-type ladder polymers", *Macromolecules*, 25 (1992) 3546–3548.
- 33 R. C. G. M. van den Schoor, R. H. M. van de Leur and J. H. W. de Wit, "Synthesis of a polypyrrole film on a non-conducting substrate: the influence of the acid concentration on the Fe^{3+} equilibria", *Synthetic Metals*, 102 (1999) 1404–1405.
- 34 F. Jonas and G. Heywang, "Technical applications for conductive polymers", *Electrochimica Acta*, 39 (1994) 1345–1347.
- 35 A. Kumar and J. R. Reynolds, "Soluble Alkyl-Substituted Poly(ethylenedioxythiophenes) as Electrochromic Materials", *Macromolecules*, 29 (1996) 7629–7630.
- 36 L. Groenendaal, F. Jonas, D. Freitag, H. Pielartzik and J. R. Reynolds, "Poly(3,4-ethylenedioxythiophene) and Its Derivatives: Past, Present, and Future", *Advanced Materials*, 12 (2000) 481–494.
- 37 U. Mitschke and P. Bäuerle, "The electroluminescence of organic materials", *Journal of Materials Chemistry*, 10 (2000) 1471–1507.
- 38 J. H. Burroughes, D. D. C. Bradley, A. R. Brown, R. N. Marks, K. Mackay, R. H. Friend, P. L. Burns and A. B. Holmes, "Light-emitting diodes based on conjugated polymers", *Nature*, 347 (1990) 539–541.
- 39 G. Grem, G. Leditzky, B. Ullrich and G. Leising, "Blue electroluminescent device based on a conjugated polymer", *Synthetic Metals*, 51 (1992) 383–389.
- 40 F. Garten, J. Vrijmoeth, A. R. Schatmann, R. E. Gill, T. M. Klapwijk and G. Hadziianou, "Light-emitting diodes based on polythiophene: influence of the metal workfunction on rectification properties" *Synthetic Metals*, 76 (1996) 85–89.
- 41 M. Uchida, Y. Ohmori, C. Morishima, K. Yoshino, "Visible and blue electroluminescent diodes utilizing poly(3-alkylthiophene)s and poly(alkylfluorene)s", *Synthetic Metals*, 57 (1993) 4168–4173.
- 42 R. H. Friend, R. W. Gymer, A. B. Holmes, J. H. Burroughes, R. N. Marks, C. Taliani, D. D. C. Bradley, D. A. Dos Santos, J. L. Bredas, M. Logdlund and W. R. Salaneck, "Electroluminescence in conjugated polymers", *Nature*, 397 (1999) 121–128.

- 43 H. Aziz and Z. D. Popovic, "Degradation Phenomena in Small-Molecule Organic Light-Emitting Devices", *Chem. Mater.* 2004, 16, 4522–4532.
- 44 J. W. Huh, Y. M. Kim, Y. W. Park, J. H. Choi, J. W. Lee, J. W. Lee, J. W. Yang, S. H. Ju, K. K. Paek, and B. K. Ju, "Characteristics of organic light-emitting diodes with conducting polymer anodes on plastic substrates", *Journal of Applied Physics*, 103 (2008) 044502.
- 45 A. Petr, F. Zhang, H. Peisert, M. Knupfer and L. Dunsch, "Electrochemical adjustment of the work function of conducting polymers", *Chemical Physics Letters*, 385 (2004) 140–143.
- 46 C. D. Dimitrakopoulos and D. J. Mascaro, "Organic thin-film transistors: A review of recent advances", *IBM Journal of Research and Development*, 45 (2001) no. 1.
- 47 M. C. Hwang, J.-W. Jang, T. K. An, C. E. Park, Y.-H. Kim and S.-K. Kwon, "Synthesis and Characterization of New Thermally Stable Poly(naphthodithiophene) Derivatives and Applications for High-Performance Organic Thin Film Transistors", *Macromolecules*, 45 (2012) 4520–4528.
- 48 J. Ficker, A. Ullmann, W. Fix, H. Rost and W. Clemens, "Stability of polythiophene-based transistors and circuits", *Journal of Applied Physics*, 94 (2003) 2638–2641.
- 49 W.-H. Lee, H. Kong, S.-Y. Oh, H.-K. Shim and I.-N. Kang, "Field-effect transistors based on PPV derivatives as a semiconducting layer", *Journal of Polymer Science Part A: Polymer Chemistry*, 47 (2009) 111–120.
- 50 E. J. Meijer, D. M. De Leeuw, S. Setayesh, E. Van Veenendaal, B.-H. Huisman, P. W. M. Blom, J. C. Hummelen, U. Scherf and T. M. Klapwijk, "Solution-processed ambipolar organic field-effect transistors and inverters", *Nature Materials*, 2 (2003) 678–682.
- 51 A. Babel, J. D. Wind and S. A. Jenekhe, "Ambipolar Charge Transport in Air-Stable Polymer Blend Thin-Film Transistors", *Advanced Functional Materials*, 14 (2004) 891–898.
- 52 J. A. Lim, J. H. Cho, Y. D. Park, D. H. Kim, M. Hwang and K. Cho, "Solvent effect of inkjet printed source/drain electrodes on electrical properties of polymer thin-film transistors", *Applied Physics Letters*, 88 (2006) 082102.
- 53 J. E. Yooa, K. S. Leeb, A. Garciac, J. Tarvera, E. D. Gomeza, K. Baldwina, Y. Sunb, H. Mengd, T.-Q. Nguyenc and Y.-L. Looa, "Directly patternable, highly conducting polymers for broad applications in organic electronics", *Proceedings of the National Academy of Sciences of the United States of America*, 170 (2010) 5712–5717.
- 54 D. Nilsson, M. Chen, T. Kugler, T. Remonen, M. Armgarth and Magnus Berggren, "Bi-stable and Dynamic Current Modulation in Electrochemical Organic Transistors", *Advanced Materials*, 14 (2002) 51–54.
- 55 S. Günes, H. Neugebauer and N. S. Sariciftci, "Conjugated Polymer-Based Organic Solar Cells", *Chemical Review*, 107 (2007) 1324–1338.

- 56 T. Bessho, S. M. Zakeeruddin, C.-Y. Yeh, E. W.-G. Diau and M. Grätzel, "Highly Efficient Mesoscopic Dye-Sensitized Solar Cells Based on Donor–Acceptor-Substituted Porphyrins", *Angewandte Chemie International Edition*, 49 (2010) 6646–6649.
- 57 J. Roncali, "Synthetic Principles for Bandgap Control in Linear π -Conjugated Systems", *Chemical Review*, 97 (1997) 173–205.
- 58 J. J. M. Halls, K. Pichler, R. H. Friend, S. C. Moratti, and A. B. Holmes, "Exciton diffusion and dissociation in a poly(*p*-phenylenevinylene)/C₆₀ heterojunction photovoltaic cell", *Applied Physical Letters*, 68 (1996) 3120–3122.
- 59 S. E. Shaheen, C. J. Brabec, N. S. Sariciftci, F. Padinger, T. Fromherz and J. C. Hummelen, "2.5% efficient organic plastic solar cells", *Applied Physical Letters*, 78 (2001) 841–843.
- 60 W. Ma, C. Yang, X. Gong, K. Lee and A. J. Heeger, "Thermally Stable, Efficient Polymer Solar Cells with Nanoscale Control of the Interpenetrating Network Morphology", *Advanced Functional Materials*, 15 (2005) 1617–1622.
- 61 K. M. Coakley and M. D. McGehee, "Conjugated Polymer Photovoltaic Cells", *Chemistry of Materials*, 16 (2004) 4533–4542.
- 62 M. Koudelka, "Performance characteristics of a planar 'Clark-type' oxygen sensor", *Sensors and Actuators*, 9 (1986) 249–258.
- 63 T. Ruzgas, E. Csöregi, J. Emnéus, L. Gorton and G. Marko-Varga, "Peroxidase-modified electrodes: Fundamentals and application", *Analytica Chimica Acta*, 330 (1996) 123–138.
- 64 M. Umana and J. Waller, "Protein-Modified Electrodes. The Glucose Oxidase/Polypyrrole System", *Analytical Chemistry*, 58 (1986) 2979–2983.
- 65 W. Trettnak, I. Liontc and M. Mascini, "Cholesterol biosensors prepared by electropolymerization of pyrrole", *Electroanalysis*, 5 (1993) 753–763.
- 66 S. Uchiyama, Y. Hasebe and M. Tanaka, "L-Ascorbate sensor with polypyrrole-coated carbon felt membrane electropolymerized in a cucumber juice solution", *Electroanalysis*, 9 (1997) 176–178.
- 67 T. Matsue, N. Kasai, M. Narumi, M. Nishizawa, H. Yamada and I. Uchida, "Electron-transfer from NADH dehydrogenase to polypyrrole and its applicability to electrochemical oxidation of NADH", *Journal of Electroanalytical Chemistry*, 300 (1991) 111–118.
- 68 R. Dobay, G. Harsányi and C. Visy, "Detection of uric acid with a new type of conducting polymer-based enzymatic sensor by bipotentiostatic technique", *Analytica Chimica Acta*, 358 (1999) 187–194.
- 69 H. Xue, Z. Shen and Y. Li, "Polyaniline–polyisoprene composite film based glucose biosensor with high permselectivity", *Synthetic Metals*, 124 (2001) 345–349.

- 70 A. Morrin, O. Ngamna, A. J. Killard, S. E. Moulton, M. R. Smyth and G. G. Wallace, "An Amperometric Enzyme Biosensor Fabricated from Polyaniline Nanoparticles", *Electroanalysis*, 17 (2005) 423–430.
- 71 A. Kros, S. W. F. M. van Hövell, N. A. J. M. Sommerdijk and R. J. M. Nolte, "Poly(3,4-ethylenedioxythiophene)-Based Glucose Biosensors", *Advanced Materials*, 13 (2001) 1555–1557.
- 72 G. Bidan, M. Billon, T. Livache, G. Mathis, A. Roget and L.M. Torres-Rodriguez, "Conducting polymers as a link between biomolecules and microelectronics", *Synthetic Metals*, 102 (1999) 1363–1365.
- 73 T. Livache, A. Roget, E. Dejean, C. Barthet, G. Bidan and R. Téoule, "Biosensing effects in functionalized electroconducting conjugated polymer layers: addressable DNA matrix for the detection of gene mutations", *Synthetic Metals*, 71 (1995) 2143–2146.
- 74 A. Ramanaviciene and A. Ramanavicius, "Pulsed amperometric detection of DNA with an ssDNA/polypyrrole-modified electrode", *Analytical and Bioanalytical Chemistry*, 379 (2004) 287–293.
- 75 F. Darain, S.-U. Park and Y.-B. Shim, "Disposable amperometric immunosensor system for rabbit IgG using a conducting polymer modified screen-printed electrode", *Biosensors and Bioelectronics*, 18 (2003) 773–780.
- 76 B. Piro, S. Reisberg, G. Anquetin, H.-T. Duc and M.-C. Pham, "Quinone-Based Polymers for Label-Free and Reagentless Electrochemical Immunosensors: Application to Proteins, Antibodies and Pesticides Detection", *Biosensors*, 3 (2013) 58–76.
- 77 J. Sutter, E. Lindner, R.E. Gyurcsányi and E. Pretsch, "A polypyrrole-based solid-contact Pb^{2+} -selective PVC-membrane electrode with a nanomolar detection limit", *Analytical and Bioanalytical Chemistry*, 380 (2004) 7–14.
- 78 J. Sutter, A. Radu, S. Peper, Eric Bakker and E. Pretsch, "Solid-contact polymeric membrane electrodes with detection limits in the subnanomolar range", *Analytica Chimica Acta*, 523 (2004) 53–59.
- 79 J. Bobacka, "Conducting Polymer-Based Solid-State Ion-Selective Electrodes", *Electroanalysis*, 18 (2006) 7–18.
- 80 R.E. Gyurcsányi, N. Rangisetty, S. Clifton, B. D. Pendley and E. Lindner, "Microfabricated ISEs: critical comparison of inherently conducting polymer and hydrogel based inner contacts", *Talanta* 63 (2004) 89–99.
- 81 M. Vázquez, J. Bobacka, Ari Ivaska and A. Lewenstam, "Influence of oxygen and carbon dioxide on the electrochemical stability of poly(3,4-ethylenedioxythiophene) used as ion-to-electron transducer in all-solid-state ion-selective electrodes", *Sensors and Actuators B*, 82 (2002) 7–13.

- 82 T. Lindfors and A. Ivaska, "Stability of the inner polyaniline solid contact layer in all-solid-state K^+ -selective electrodes based on the plasticized poly(vinyl chloride)", *Analytical Chemistry*, 76 (2004) 4387–4394.
- 83 T. Blaz, J. Migdalski and A. Lewenstam, "Junction-less reference electrode for potentiometric measurements obtained by buffering pH in a conducting polymer matrix", *Analyst*, 130 (2005) 637–643.
- 84 A. Kisiel, H. Marcisz, A. Michalska and K. Maksymiuk, "All-solid-state reference electrodes based on conducting polymers", *Analyst*, 130 (2005) 1655–1662.
- 85 P. Hodge, G. A. Power and M. A. Rabjohns, "Synthesis of poly(anthracene-2,6-diyl) and a copolymer containing alternately anthracene-2,6-diyl and p-phenylene units", *Chemical Communications*, 1 (1997) 73–74.
- 86 T. M. Figueira-Duarte, P. G. Del Rosso, R. Trattnig, S. Sax, E. J. W. List and K. Müllen, "Designed suppression of aggregation in polypyrene: toward high-performance blue-light-emitting diodes", *Advanced Materials*, 22 (2010) 990–993.
- 87 R. C. West (Editor-in-Chief), "Fused Polycyclic Hydrocarbons" in *CRC Handbook of Chemistry and Physics*, 67th edition (1986–1987).
- 88 X. Feng, W. Pisula and K. Müllen, "Large polycyclic aromatic hydrocarbons: synthesis and discotic organization", *Pure and Applied Chemistry*, 81 (2009) 2203–2224.
- 89 K. Ravindra, R. Sokhi and R. Van Grieken, "Atmospheric polycyclic aromatic hydrocarbons: Source attribution, emission factors and regulation", *Atmospheric Environment*, 42 (2008) 2895–2921.
- 90 J. Jacob, "The significance of polycyclic aromatic hydrocarbons as environmental carcinogens", *Pure and Applied Chemistry*, 68 (1996) 301–308.
- 91 M. Tommasini, C. Castiglioni and G. Zerbi, "Raman scattering of molecular graphenes", *Physical Chemistry Chemical Physics*, 11 (2009) 10185–10194.
- 92 D. J. Cook, S. Schlemmer, N. Balucani, D. R. Wagner, B. Steiner and R. J. Saykally, "Infrared emission spectra of candidate interstellar aromatic molecules", *Nature* 380 (1996) 227–229.
- 93 K. Tanemura, T. Suzuki and T. Horaguchi, "Synthesis of sulfonated polynaphthalene, polyanthracene, and polypyrene as strong solid acids via oxidative coupling polymerization", *Journal of Applied Polymer Science*, 127 (2013) 4524–4536.
- 94 J. M. Reyna-González, M. Aguilar-Martínez, A. García-Concha, C. Palomar and E. Rivera, "A comparative investigation between poly(1-ethynylpyrene) and poly(1,6-(3-ethynylpyrenylene)): Influence of the structure on the thermal, optical, electrochemical properties and conductivity", *Synthetic Metals*, 159 (2009) 659–665.
- 95 T. S. Totton, A. J. Misquitta and M. Kraft, "A quantitative study of the clustering of polycyclic aromatic hydrocarbons at high temperatures", *Physical Chemistry Chemical Physics*, 14 (2012) 4081–4094.

- 96 D. Adam, P. Schuhmacher, J. Simmerer, L. Häussling, K. Siemensmeyer, K. H. Etzbach, H. Ringsdorf and D. Haarer, "Fast photoconduction in the highly ordered columnar phase of a discotic liquid crystal", *Nature*, 371 (1994) 141–143.
- 97 M. Deetlefs, K. R. Seddon and M. Shara, "Predicting physical properties of ionic liquids", *Physical Chemistry Chemical Physics*, 8 (2006) 642–649.
- 98 P. Bonhôte, A.-P. Dias, N. Papageorgiou, K. Kalyanasundaram and M. Grätzel, "Hydrophobic, Highly Conductive Ambient-Temperature Molten Salts", *Inorganic Chemistry*, 35 (1996) 1168–1178.
- 99 A. S. Larsen, J. D. Holbrey, F. S. Tham and C. A. Reed, "Designing Ionic Liquids: Imidazolium Melts with Inert Carborane Anions", *Journal of The American Chemical Society*, 122 (2000) 7264–7272.
- 100 M. Galiński, A. Lewandowski and I. Stępnik, "Ionic liquids as electrolytes", *Electrochimica Acta*, 51 (2006) 5567–5580.
- 101 M. J. Earle, J. M. S. S. Esperança, M. A. Gilea, J. N. Canongia Lopes, L. P. N. Rebelo, J. W. Magee, K. R. Seddon and J. A. Widegren, "The distillation and volatility of ionic liquids", *Nature*, 439 (2006) 831–834.
- 102 M. Matzke, S. Stolte, K. Thiele, T. Juffernholz, J. Arning, J. Ranke, U. Welz-Biermann and B. Jastorff, "The influence of anion species on the toxicity of 1-alkyl-3-methylimidazolium ionic liquids observed in an (eco)toxicological test battery", *Green Chemistry*, 9 (2007) 1198–1207.
- 103 N. Koura, H. Ejiri and K. Takeishi, "Polyaniline Secondary Cells with Ambient Temperature Molten Salt Electrolytes", *Journal of The Electrochemical Society*, 140 (1993) 602–605.
- 104 F. E. Kühn, J. Zhao, M. Abrantes, W. Sun, C. A. M. Afonso, L. C. Branco, I. S. Gonçalves, M. Pillinger and C. C. Romão, "Catalytic olefin epoxidation with cyclopentadienyl-molybdenum complexes in room temperature ionic liquids", *Tetrahedron Letters*, 46 (2005) 47–52.
- 105 U. Schröder, J. D. Wadhawan, R. G. Compton, F. Marken, P. A. Z. Suarez, C. S. Consorti, R. F. de Souza and J. Dupont, "Water-induced accelerated ion diffusion: voltammetric studies in 1-methyl-3-[2,6-(S)-dimethylocten-2-yl] imidazolium tetrafluoroborate, 1-butyl-3-methylimidazolium tetrafluoroborate and hexafluorophosphate ionic liquids", *New Journal of Chemistry*, 24 (2000) 1009–1015.
- 106 K. Sekiguchi, M. Atobe and T. Fuchigami, "Electrooxidative polymerization of aromatic compounds in 1-ethyl-3-methylimidazolium trifluoromethanesulfonate room-temperature ionic liquid", *Journal of Electroanalytical Chemistry*, 557 (2003) 1–7.
- 107 P. Damlin, C. Kvarnström and A. Ivaska, "Electrochemical synthesis and in situ spectroelectrochemical characterization of poly(3,4 ethylenedioxythiophene) (PEDOT) in room temperature ionic liquids", *Journal Electroanalytical Chemistry*, 570 (2004) 113–122.

- 108 K. Wagner, J. M. Pringle, S. B. Hall, M. Forsyth, D. R. MacFarlane and D. L. Officer, "Investigation of the electropolymerisation of EDOT in ionic liquids", *Synthetic Metals*, 153 (2005) 257–260.
- 109 K. Sekiguchi, M. Atobe and T. Fuchigami, "Electropolymerization of pyrrole in 1-ethyl-3-methylimidazolium trifluoromethanesulfonate room temperature ionic liquid", *Electrochemistry Communications*, 4 (2002) 881–885.
- 110 J. M. Pringle, J. Efthimiadis, P. C. Howlett, J. Efthimiadis, D. R. MacFarlane, A. B. Chaplin, S. B. Hall, D. L. Officer, G. G. Wallace and M. Forsyth, "Electrochemical synthesis of polypyrrole in ionic liquids", *Polymer*, 45 (2004) 1447–1453.
- 111 J. M. Pringle, M. Forsyth, D. R. MacFarlane, K. Wagner, S. B. Hall and D. L. and Officer, "The influence of the monomer and the ionic liquid on the electrochemical preparation of polythiophene", *Polymer*, 46, (2005) 2047–2058.
- 112 H. Neugebauer, "In situ vibrational spectroscopy of conducting polymer electrodes", *Macromolecular Symposia*, 94 (1995) 61–73.
- 113 B. A. Boukamp, "A nonlinear least squares fit procedure of immittance data of electrochemical systems", *Solid State Ionics*, 20 (1986) 31–44.
- 114 F. M. Smits, "Measurement of Sheet Resistivities with the Four-Point Probe", *The Bell System Technical Journal*, 37 (1958) 711–718.
- 115 J. Kankare and E.-L. Kupila, "In-situ conductance measurement during electropolymerization", *Journal of Electroanalytical Chemistry*, 322 (1992) 167–181.
- 116 J. Bobacka, A. Ivaska and A. Lewenstam, "Potentiometric Ion Sensors", *Chemical Reviews*, 108 (2008) 329–351.
- 117 R. D. Piner, J. Zhu, F. Xu, S. Hong and C. A. Mirkin, "(“Dip-Pen” Nanolithography)", *Science*, 283 (1999) 661–663.
- 118 B. L. Weeks, M. W. Vaughn and J. J. DeYoreo, "Direct Imaging of Meniscus Formation in Atomic Force Microscopy Using Environmental Scanning Electron Microscopy", *Langmuir*, 21 (2005) 8096–8098.
- 119 H.-T. Wang, O. A. Nafday, J. R. Haaheim, E. Tevaarwerk, N. A. Amro, R. G. Sanedrin, C.-Y. Chang, F. Ren and S. J. Pearton, "Toward conductive traces: Dip Pen Nanolithography of silver nanoparticle-based inks", *Applied Physical Letters*, 93 (2008) 143105.
- 120 D. S. Ginger, H. Zhang, and C. A. Mirkin, "The Evolution of Dip-Pen Nanolithography", *Angewandte Chemie International Edition*, 43 (2004) 30–45.
- 121 M. Yang, P. E. Sheehan, W. P. King and L. J. Whitman, "Direct Writing of a Conducting Polymer with Molecular-Level Control of Physical Dimensions and Orientation", *Journal of the American Chemical Society*, 128 (2006) 6774–6775.
- 122 H.-H. Lu, C.-Y. Lin, T.-C. Hsiao, Y.-Y. Fang, K.-C. Ho, D. Yang, C.-K. Lee, S.-M. Hsu and C.-W. Lin, "Electrical properties of single and multiple poly(3,4-ethylenedioxythiophene) nanowires for sensing nitric oxide gas", *Analytica Chimica Acta* 640 (2009) 68–74.

- 123 H. Nakashima, M. J. Higgins, C. D. O'Connell, K. Torimitsu, G. G. Wallace , "Liquid Deposition Patterning of Conducting Polymer Ink onto Hard and Soft Flexible Substrates via Dip-Pen Nanolithography", *Langmuir* 28 (2012) 804–811.
- 124 C. Gao and D. Yan, "Hyperbranched polymers: from synthesis to applications", *Progress in Polymer Science*, 29 (2004) 183–275.
- 125 P. J. Pearce and A. J. Bard, "Polymer Films on Electrodes. II. Film Structure and Mechanism of Electron Transfer with Electrodeposited Poly(vinylferrocene)", *Journal of Electroanalytical Chemistry*, 112 (1980) 97–115.
- 126 K. Suzuki, "Novel Lewis acid catalysis in organic synthesis", *Pure and Applied Chemistry*, 66 (1994) 1557–1564.
- 127 P. Hapiot and C. Lagrost, "Electrochemical Reactivity in Room-Temperature Ionic Liquids", *Chemical Review*, 108 (2008) 2294–2299.
- 128 C. Castiglioni, M. Gussoni and G. Zerbi, "Amplitude mode theory and classical molecular dynamics: The interpretation of the vibrational infrared and Raman spectra of polyparaphenylene", *Synthetic Metals*, 29 (1989) 1–6.
- 129 H. Ohtsuka, Y. Furukawa and M. Tasumi, "Dependencies of the Raman spectra of *p*-oligophenyls on the chain length and the excitation wavelength", *Spectrochimica Acta*, 49 (1993) 731–737.
- 130 R. C. Doss and P. W. Solomon, "Infrared Spectra and Synthesis of Some Polyphenyls", *The Journal of Organic Chemistry*, 29 (1964) 1567–1574.
- 131 D. Talbi and G. S. Chandler, "Theoretical infrared spectra of biphenyl, terphenyls and tetraphenyls for astrophysical purposes", *Journal of Molecular Spectroscopy*, 275 (2012) 21–27.
- 132 D. M. de Leeuw, M. M. J. Simenon, A. R. Brown and R. E. F. Einerhand, "Stability of n-type doped conducting polymers and consequences for polymeric microelectronic devices", *Synthetic Metals*, 87 (1997) 53–59.
- 133 G. Horowitz, "Organic Field-Effect Transistors", *Advanced Materials*, 10 (1998) 365–337.
- 134 T. Yohannes, H. Neugebauer, S. Luzzati, M. Catellani, S. A. Jenekhe and N. S. Sariciftci, "Multiple Electrochemical Doping Induced Insulator-to-Conductor Transitions Observed in Conjugated Ladder Polymer Polybenzimidazobenzophenanthroline (BBL)", *Journal of Physical Chemistry B*, 104 (2000) 9430–9437.
- 135 R. Rieger and K. Müllen, "Forever young: polycyclic aromatic hydrocarbons as model cases for structural and optical studies", *Journal of Physical Organic Chemistry*, 23 (2010) 315–325.
- 136 M. A. Pimenta, G. Dresselhaus, M. S. Dresselhaus, L. G. Cancado, A. Jorio and R. Saito, "Studying disorder in graphite-based systems by Raman spectroscopy", *Physical Chemistry Chemical Physics*, 9 (2007) 1276–1291.

- 137 G. Lisak, J. Bobacka and A. Lewenstam, "Recovery of nanomolar detection limit of solid-contact lead (II)-selective electrodes by electrode conditioning", *Journal of Solid State Electrochemistry*, 16 (2012) 2983–2991.
- 138 M. Berggren and A. Richter-Dahlfors, "Organic Bioelectronics", *Advanced Materials*, 19 (2007) 3201–3213.
- 139 S. Ghosh and O. Inganäs, "Electrochemical Characterization of Poly(3,4-ethylene dioxythiophene) Based Conducting Hydrogel Networks", *Journal of the Electrochemical Society*, 147 (2000) 1872–1877.
- 140 X. Crispin, S. Marciniak, W. Osikowicz, G. Zotti, A. W. Denier van der Gon, F. Louwet, M. Fahlman, L. Groenedaal, F. De Schryver and W. R. Salaneck, "Conductivity, morphology, interfacial chemistry, and stability of poly(3,4-ethylene dioxythiophene)–poly(styrene sulfonate): A photoelectron spectroscopy study", *Journal of Polymer Science Part B: Polymer Physics*, 41 (2003) 2561–2583.
- 141 M. Döbbelin, R. Marcilla, C. Tollan, J. A. Pomposo, J.-R. Sarasua and D. Mecerreyes, "A new approach to hydrophobic and water-resistant poly(3,4-ethylenedioxythiophene) poly(styrenesulfonate) films using ionic liquids", *Journal of Materials Chemistry*, 18 (2008) 5354–5358.
- 142 A. M. Nardes, R. A. J. Janssen and M. Kemerink, "A Morphological Model for the Solvent-Enhanced Conductivity of PEDOT:PSS Thin Films", *Advanced Functional Materials*, 18 (2008) 865–871.
- 143 S. Rozhok, R. Piner, C. A. Mirkin, "Dip-Pen Nanolithography: What Controls Ink Transport?", *Journal of Physical Chemistry*, 107 (2003) 751–757.



ISBN 978-952-12-2977-0

Painosalama Oy – Turku, Finland 2013